Hindawi
Mathematical Problems in Engineering
Volume 2020, Article ID 4164526, 30 pages
https://doi.org/10.1155/2020/4164526

*Research Article*

# Deadbeat-Based Model Predictive Voltage Control for a Sensorless Five-Phase Induction Motor Drive

**Mahmoud A. Mossa**,[1] **Nguyen Vu Quynh**,[2] **Hamdi Echeikh**,[3] **and Ton Duc Do**[4]

[1]*Electrical Engineering Department, Faculty of Engineering, Minia University, Minia 61111, Egypt*
[2]*Electrical and Electronics Department, Lac Hong University, Dong Nai, Vietnam*
[3]*Department of Electrical Engineering, National Engineering School of Monastir, P.O. Box 5035, Monastir, Tunisia*
[4]*Department of Robotics and Mechatronics, School of Engineering and Digital Sciences (SEDS), Nazarbayev University, Nur-Sultan Z05H0P9, Kazakhstan*

Correspondence should be addressed to Mahmoud A. Mossa; mahmoud_a_mossa@mu.edu.eg and Nguyen Vu Quynh; vuquynh@lhu.edu.vn

Received 16 April 2020; Accepted 11 June 2020; Published 15 July 2020

Academic Editor: Salvatore Strano



This paper introduces a direct model predictive voltage control (DMP VC) for a sensorless five-phase induction motor drive. The operation of the proposed sensorless DMP VC is based on the direct control of the applied stator voltages instead of controlling the torque and flux as in model predictive direct torque control (MP DTC). Thus, the simplicity of the control system is enhanced, which saves the computational time and reduces the commutation losses as well. The methodology based on which the proposed sensorless DMP VC performs its operation depends on minimizing a cost function that calculates the error between the reference and actual values of the direct and quadrature ($d$-$q$) axes components of stator voltages. The reference values of $d$-$q$ components of stator voltages are obtained through incorporating the deadbeat control within the proposed model predictive system. A robust back-stepping observer is proposed for estimating the speed, stator currents, rotor flux, and rotor resistance. The validity of the proposed sensorless DMP VC is confirmed through performing detailed and extensive comparisons between the proposed DMP VC and MP DTC approach. The obtained results state that the drive is exhibiting better performance under the proposed DMP VC with less ripples content and reduced computational burden. Moreover, the proposed back-stepping observer has confirmed its effectiveness in estimating the speed and other variables for a wide range of speed operation.

## 1. Introduction

Recently, the multiphase machine drives have been given great concern due to their various advantages compared with the three-phase AC machine drives [1–3]. These advantages can be addressed in the form of high robustness, smooth torque profile, reduced ripples content in the controlled variables, reduced current rating for each phase of the stator, and enhanced fault-ride through capability [4–6]. All of these merits have motivated the industrial communities to use the multiphase machines in high-power applications such as aircraft and naval propulsion and electric traction systems, as well as aerospace applications [7–9].

One of the most familiar types of multiphase machines is the five-phase induction motor (FPIM) [10–12]. Many control topologies have been presented for controlling the operation of the FPIM drives so that an optimal performance can be obtained from the drive in terms of low ripple contents, high efficiency, and ease of practical implementation. The direct torque control (DTC) and field oriented control (FOC) are considered as the most used control topologies for the majority of electric machine drives [13–16]. Both techniques have contributed effectively to improving the dynamic performance of the FPIM drive, but on the other hand they have suffered from some problems. For example, for the FOC approach, the system complexity

is obvious due to the utilization of multiple proportional-integral (PI) controllers, which require precise tuning of its coefficients. This is in addition to the time delay, which is added to the system response due to the use of PI controllers [13, 14]. On the other hand, the DTC control approach has managed to reduce the system complexity and achieve fast dynamic response as well. However, it has suffered from the remarkable ripples content in the controlled variables [15, 16].

To overcome the shortages of the DTC and FOC approaches, the model predictive control (MPC) principle has been presented for the FPIM drive in different forms. Some of these forms have depended on controlling the torque and flux and were entitled as model predictive direct torque control (MP DTC) [12, 17]. The MP DTC approach has succeeded in reducing the system complexity and reducing the ripples compared with the classic DTC look-up table based approach, but the ripples have not been totally suppressed.

However, the MP DTC has suffered from the high computational burden, which cannot be realized by all microprocessors. The main factor that manages the computation time in the model predictive control in general is the form and parts of the used cost function. For example, for the MP DTC, the cost function is consisting of two parts: one for the torque regulation and the other for the flux management. This function type requires the utilization of a weighting factor to weigh the importance of each term with respect to the other. The calculation of optimal weighting factor is a time-consuming process, which results in adding extra execution time and increasing the commutation losses. This is in addition to the fact that both terms (torque and flux) need to be estimated, which again lengthens the computational time for each cycle.

As a solution for these issues, the current paper proposes a direct model predictive voltage control (DMP VC) approach for a sensorless FPIM drive. The operation of the proposed approach is based upon utilizing a cost function form, which consists of two similar terms to avoid using a weighting factor. The two similar terms of the cost function are the errors between the reference values of direct-quadrature ($d$-$q$) axes components of stator voltage and their correspondent actual values. Through checking the cost function configuration as will be illustrated later, it can be realized that the cost function's variables (the voltages applied to the motor terminals) can be directly accessed without performing any estimation. This procedure has resulted in reducing the calculation time of the cost function, which reduces the commutation time as well as switching power losses. Moreover, the control is now dealing directly with the fastest variable to be applied to the PFIM (which is here the stator voltage), and this results in enhancing the system dynamic response.

To increase the robustness of the FPIM drive, several sensorless schemes have been proposed for estimating the rotor speed and rotor flux. Some of them have depended on utilizing the model reference adaptive system (MRAS) observer [18–20]. The main deficiency of the MRAS observer is the sensitivity to parameters variation, especially at low speed operation. Other sensorless schemes have utilized the sliding mode observer [21, 22]. The precision of the speed estimation using the sliding mode observers has been negatively affected by the noise characteristics. Moreover, in order to solve the chattering problem, higher-order sliding modes have been utilized, which resulted in increasing the system's complexity. Another senseless procedure has implemented the extended Kalman filter for estimating the speed [23]. The main issue related to this scheme is the dependency of the observer's model on the parameters, which can result in deteriorating the estimation due to the parameters variation under certain operating conditions. Another scheme has depended on estimating the rotor position through tracking the saliency position [24]. This method has suffered from the increased computational capacity of the system due to the system complexity.

As an attempt to achieve robust and precise speed estimation without adding extra computational burden on the controller, a new back-stepping speed observer is presented in this paper. The proposed back-stepping observer not only estimates the speed but also estimates the stator current, the rotor flux, and rotor resistance. Checking the observer's stability has been presented to confirm its effectiveness in estimating the speed precisely for a wide range of operations under varying the rotor resistance. It is worth mentioning that the back-stepping principle has been introduced for different AC machine drives as a control system [25, 26], but it has been rarely utilized as a speed observer.

The back-stepping approach is a recursive procedure, the operation of which is based on the Lyapunov theory. This strategy is widely used for designing the control laws for uncertain systems. To our knowledge, majority of the methods that have been used for observing the states of the induction machine depending on the back-stepping principle and introduced in the literature have been mainly utilized for estimating the resistive and inductive parameters of the machine in the presence of mechanical speed sensor. However, the difficulties are coming out when eliminating the speed sensor because of the unobservability of the motor, especially at very low speed. It is shown that the proposed method in [27] must be modified to take into account this nonlinear dynamic coupling by introducing other damping terms into each control input. The second contribution that the paper presents is to apply the back-stepping observer to the systems that have high degree of coupling between the electromagnetic and mechanical variables. In this form, the nonlinearities entering each subsystem are allowed to depend on the output associated with the subsystem and the states of the upper subsystem, including the unmeasured ones. The proposed observer algorithm is applied to the five-phase induction motor. The proposed observer only takes the stator voltages and currents as inputs and provides the speed, the rotor flux, the stator current, and rotor resistances as estimated outputs.

The paper is organized as follows; it starts with introducing the mathematical model of the five-phase IM (FPIM) drive. Then, in Section 3, the proposed DMP VC approach is described and analyzed in detail. After that, in Section 4, the proposed back-stepping observer is presented and

explained. In Section 5, the complete system configuration is presented. In Section 6, the test results are introduced and discussed. The test results are presented in the form of comprehensive comparisons between the proposed DMP VC and MP DTC approach. Finally, Section 7 introduces the conclusion and the outcomes of the paper.

The contributions of the paper can be addressed through the following items:

(i) The proposed DMP VC approach has not been tested before with the FPIM drive.

(ii) The derivation and analysis of the proposed DMP VC are performed through a detailed mathematical verification so that the base principle can be easily understood.

(iii) The proposed back-stepping observer has been presented and analyzed in detail so that the operation principles of the observer can be easily verified.

(iv) The robustness of the proposed back-stepping observer has been verified under the parameters variation for a wide range of speed operation.

(v) A detailed comparison between the proposed DMP VC and MP DTC for the FPIM drive is carried out in terms of the total harmonic distortion (THD) for the current signals and in terms of the average error values. Moreover, a comparison has been carried out in terms of switching frequencies and number of commutations and finally in terms of the computational time and switching losses.

## 2. Mathematical Model of FPIM

Several studies have presented and formulated the mathematical model of FPIM according to specific assumptions [28, 29]. The model can be represented in different reference frames, such as the rotating synchronous reference frame, which gives the ($d$-$q$-$x$-$y$) axes configuration, while representing the model in the stationary reference frame gives the ($\alpha$-$\beta$-$z_1$-$z_2$) axes configuration.

When representing the FPIM model in the synchronous reference frame, the $d$-$q$ components will be responsible for managing the flux and torque, respectively. Meanwhile, the $x$-$y$ components will be responsible for developing the losses.

Under rotor field oriented control (RFOC), the following discretized relationships are obtained at instant kTs as follows:

$$\begin{aligned} \psi_{dr,k}^{rf} &= \left|\overline{\psi}_{r,k}^{rf}\right|, \\ \psi_{qr,k}^{rf} &= 0.0, \end{aligned} \tag{1}$$

where $T_s$ is the sampling time; $\psi_{dr,k}^{rf}$ and $\psi_{qr,k}^{rf}$ refer to the direct and quadrature axes components of stator flux defined in the synchronous rotating frame. Moreover, the superscript "rf" is used to state that the variables are defined in a reference frame, which rotates synchronously with the rotor flux.

Utilizing (1) and via adopting the principles of RFOC, the equations that describe the electric dynamics of the FPIM can be represented in the ($d$-$q$-$x$-$y$) reference frame by

$$\frac{d\psi_{dr,k}^{rf}}{dt} = \frac{d\overline{\psi}_{r,k}^{rf}}{dt} = \frac{L_m}{\tau_r} i_{ds,k}^{rf} - \frac{\psi_{dr,k}^{rf}}{\tau_r}, \tag{2}$$

$$\frac{d\psi_{qr,k}^{rf}}{dt} = 0.0 = \frac{L_m}{\tau_r} i_{qs,k}^{rf} - \omega_{sl,k}\psi_{dr,k}^{rf}, \tag{3}$$

$$\frac{di_{ds,k}^{rf}}{dt} = \gamma_1 i_{ds,k}^{rf} + \omega_{me,k} i_{qs,k}^{rf} + \gamma_2 \psi_{dr,k}^{rf} + \frac{1}{L_t} u_{ds,k}^{rf}, \tag{4}$$

$$\frac{di_{qs,k}^{rf}}{dt} = \gamma_1 i_{qs,k}^{rf} - \omega_{me,k} i_{ds,k}^{rf} + \gamma_2 \psi_{dr,k}^{rf} + \frac{1}{L_t} u_{qs,k}^{rf}, \tag{5}$$

$$\frac{di_{xs,k}^{rf}}{dt} = \frac{-R_s}{L_{ls}} i_{xs,k}^{rf} + \frac{1}{L_{ls}} u_{xs,k}^{rf}, \tag{6}$$

$$\frac{di_{ys,k}^{rf}}{dt} = \frac{-R_s}{L_{ls}} i_{ys,k}^{rf} + \frac{1}{L_{ls}} u_{ys,k}^{rf}, \tag{7}$$

$$\frac{d\omega_{me,k}}{dt} = \gamma_3 \psi_{dr,k}^{rf} i_{qs,k}^{rf} - \frac{p}{J} T_{l,k}, \tag{8}$$

where the subscripts $s$ and $r$ refer to the stator and rotor variables, respectively, and

$$\begin{aligned} \gamma_1 &= \frac{L_m^2 R_r + L_r^2 R_s}{L_t L_r^2}, \\ \gamma_2 &= \frac{L_m R_r}{L_t L_r}, \\ \gamma_3 &= \frac{p^2 L_m}{J L_r}, \\ \omega_{sl} &= \omega_{\overline{\psi}_r} - \omega_{me}, \end{aligned} \tag{9}$$

where $\omega_{\overline{\psi}_r}$ is the angular frequency of the rotor flux, $\omega_{me}$ is the mechanical angular frequency, and $\omega_{sl}$ is the slip angular frequency. The parameters $R_s$ and $R_r$ refer to the stator and rotor resistances, respectively. The inductances $L_s$, $L_r$, $L_m$, and $L_{ls}$ refer to the stator, rotor, magnetizing, and stator leakage inductances, respectively. The inductance $L_t = \sigma L_s$ refers to the stator transient inductance, while the constant $\sigma = 1 - (L_m^2/L_s L_r)$ refers to the total leakage factor. The parameters $p$ and $J$ refer to the pole pairs and the moment of inertia, respectively. Finally, $\tau_r = L_r/R_r$ refers to the rotor time constant.

Via utilizing the relationships (2) to (8), the equivalent circuit of the FPIM can be represented as shown in Figure 1. In this figure, it can be noticed that the model is consisting of decoupled $d$-$q$ axes equivalent circuits similar to those of three-phase IM, decoupled $x$-$y$ axes equivalent circuits, and decoupled $x$-$y$ axes equivalent circuits for the rotor. The latter can be simply represented by resistive-inductive circuits.

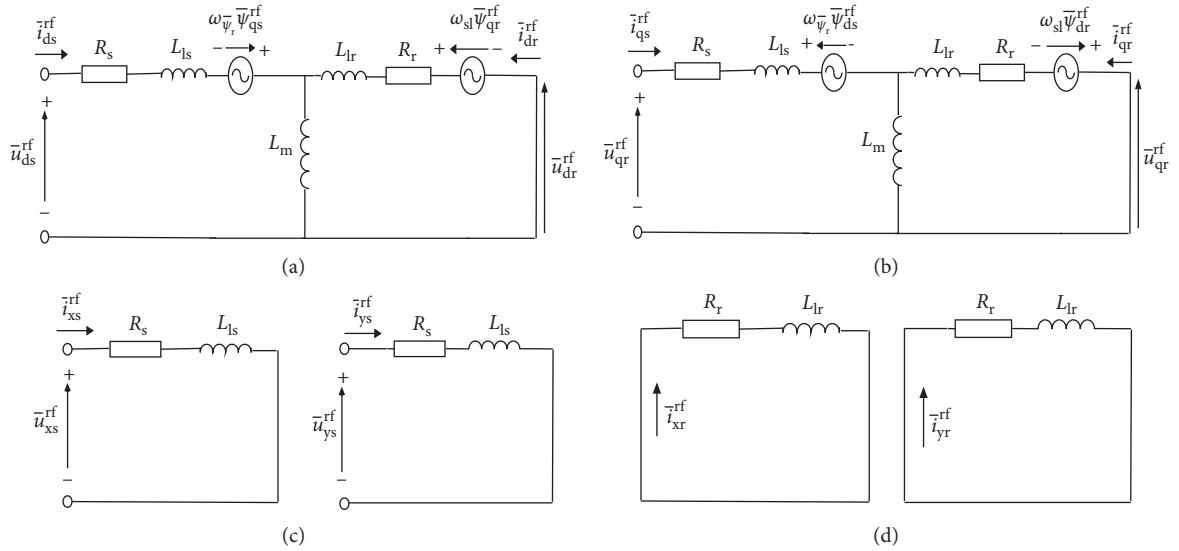


Figure 1: ($d$-$q$-$x$-$y$) axes equivalent circuit model of FPIM defined in synchronous reference frame. (a) $d$-axis equivalent circuit, (b) $q$-axis equivalent circuit, (c) $x$-$y$ axes equivalent circuits for stator side, and (d) $x$-$y$ axes equivalent circuits for rotor side.

## 3. The Proposed DMP VC Approach

The principle based upon which the proposed DMP VC approach is formulated states that the motor's flux and torque can be directly controlled via controlling the direct and quadrature ($d$-$q$) axes components of applied stator voltage ($u^{\mathrm{rf}}_{\mathrm{ds,k}}, u^{\mathrm{rf}}_{\mathrm{qs,k}}$), respectively. This argument can be verified mathematically as follows.

Under RFOC, the total rotor flux is aligned with the $d$-axis of the rotating reference frame, and the following relationships are obtained:

$$\overline{\psi}^{\mathrm{rf}}_{\mathrm{r,k}} = L_r \overline{i}^{\mathrm{rf}}_{\mathrm{r,k}} + L_m \overline{i}^{\mathrm{rf}}_{\mathrm{s,k}} = L_m \overline{i}^{\mathrm{rf}}_{\mathrm{mr,k}}, \tag{10}$$

where $\overline{i}^{\mathrm{rf}}_{\mathrm{mr,k}}$ is the rotor magnetizing current and $\overline{i}^{\mathrm{rf}}_{\mathrm{s,k}}$ and $\overline{i}^{\mathrm{rf}}_{\mathrm{r,k}}$ are the stator and rotor current vectors, respectively.

The relationship between the stator, rotor, and magnetizing currents can be represented by

$$\overline{i}^{\mathrm{rf}}_{\mathrm{mr,k}} = \frac{\overline{\psi}^{\mathrm{rf}}_{\mathrm{r,k}}}{L_{\mathrm{m}}} = \frac{L_{\mathrm{r}}}{L_{\mathrm{m}}} \overline{i}^{\mathrm{rf}}_{\mathrm{r,k}} + \overline{i}^{\mathrm{rf}}_{\mathrm{s,k}}. \tag{11}$$

Under the RFOC, the reference frame rotates with an angular speed defined by

$$\omega_{\overline{\psi}_{\mathrm{r,k}}} = \omega_{\mathrm{me,k}} + \frac{\overbrace{i^{\mathrm{rf}}_{\mathrm{qs,k}}}^{\omega_{\mathrm{sl,k}}}}{\tau_{\mathrm{r}} \overline{i}^{\mathrm{rf}}_{\mathrm{mr,k}}}. \tag{12}$$

The space vector representation under the application of RFOC is illustrated in Figure 2, through which it is observed that the total rotor flux is fixed with the $d$-axis of the rotating frame and rotates with an angular frequency of $\omega_{\overline{\psi}_{\mathrm{r,k}}}$. The angle $\delta_{\mathrm{k}}$ refers to the load angle (torque angle) between the rotor flux and stator current vectors. The stator current vector rotates with an angular frequency of $\omega_{\mathrm{s,k}} = \mathrm{d}/\mathrm{d}t\,(\delta_{\mathrm{k}} + \theta_{\overline{\psi}_{\mathrm{r,k}}})$.

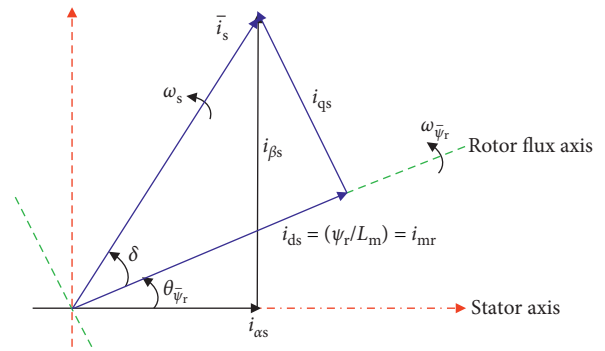


Figure 2: Vector diagram for steady-state operation of IM under RFOC.

The voltage balance in the FPIM circuit can be expressed in an alternative form by the following relationships:

$$\overline{u}^{\mathrm{rf}}_{\mathrm{s,k}} = R_{\mathrm{s}} \overline{i}^{\mathrm{rf}}_{\mathrm{s,k}} + \frac{\mathrm{d}\overline{\psi}^{\mathrm{rf}}_{\mathrm{s,k}}}{\mathrm{d}t} + j\omega_{\overline{\psi}_{\mathrm{r,k}}} \overline{\psi}^{\mathrm{rf}}_{\mathrm{s,k}}, \tag{13}$$

$$\overline{u}^{\mathrm{rf}}_{\mathrm{r,k}} = 0 = R_{\mathrm{r}} \overline{i}^{\mathrm{rf}}_{\mathrm{r,k}} + \frac{\mathrm{d}\overline{\psi}^{\mathrm{rf}}_{\mathrm{r,k}}}{\mathrm{d}t} + j\overbrace{\left(\omega_{\overline{\psi}_{\mathrm{r,k}}} - \omega_{\mathrm{me,k}}\right)}^{\omega_{\mathrm{sl,k}}} \overline{\psi}^{\mathrm{rf}}_{\mathrm{r,k}}. \tag{14}$$

By substituting (11) and (12) into (13) and (14), and after mathematical derivations, this results in

$$u^{\mathrm{rf}}_{\mathrm{ds,k}} = R_{\mathrm{s}} i^{\mathrm{rf}}_{\mathrm{ds,k}} + (1-\sigma) L_{\mathrm{s}} \frac{\mathrm{d}\overline{i}^{\mathrm{rf}}_{\mathrm{mr,k}}}{\mathrm{d}t} + \sigma L_{\mathrm{s}} \left( \frac{\mathrm{d}i^{\mathrm{rf}}_{\mathrm{ds,k}}}{\mathrm{d}t} - i^{\mathrm{rf}}_{\mathrm{qs,k}} \omega_{\overline{\psi}_{\mathrm{r,k}}} \right), \tag{15}$$

$$u^{\mathrm{rf}}_{\mathrm{qs,k}} = R_{\mathrm{s}} i^{\mathrm{rf}}_{\mathrm{qs,k}} + (1-\sigma) L_{\mathrm{s}} \overline{i}^{\mathrm{rf}}_{\mathrm{mr,k}} \omega_{\overline{\psi}_{\mathrm{r,k}}} + \sigma L_{\mathrm{s}} \left( \frac{\mathrm{d}i^{\mathrm{rf}}_{\mathrm{qs,k}}}{\mathrm{d}t} + i^{\mathrm{rf}}_{\mathrm{ds,k}} \omega_{\overline{\psi}_{\mathrm{r,k}}} \right), \tag{16}$$

$$\tau_r \frac{d\bar{i}^{rf}_{mr,k}}{dt} + \bar{i}^{rf}_{mr,k} = i^{rf}_{ds,k}, \tag{17}$$

$$\frac{J}{p}\frac{d\omega_{me,k}}{dt} = \overbrace{\underbrace{1.5p(1-\sigma)L_s}_{\nabla}\bar{i}^{rf}_{mr,k}i^{rf}_{qs,k}}^{T_{e,k}} - T_{l,k}. \tag{18}$$

Using (17) and its derivative, by substituting into (15), this results in

$$u^{rf}_{ds,k} = \sigma L_s\tau_r\frac{d^2\bar{i}^{rf}_{mr,k}}{dt^2} + \left(R_s\tau_r + L_s\right)\frac{d\bar{i}^{rf}_{mr,k}}{dt} + R_s\bar{i}^{rf}_{mr,k} - \sigma L_s i^{rf}_{qs,k}\omega_{\bar{\psi}_{r,k}}. \tag{19}$$

By taking the Laplace transform of (19), this results in

$$u^{rf}_{ds,k}(s) = \sigma L_s\tau_r\left(s^2\bar{i}^{rf}_{mr,k}(s)\right) + \left(R_s\tau_r + L_s\right)s\bar{i}^{rf}_{mr,k}(s) + R_s\bar{i}^{rf}_{mr,k}(s) - \sigma L_s\mathscr{L}\left(i^{rf}_{qs,k}\omega_{\bar{\psi}_{r,k}}\right), \tag{20}$$

where $\mathscr{L}$ denotes Laplace transform. Then the value of $\bar{i}^{rf}_{mr,k}(s)$ can be derived from (20) by

$$\bar{i}^{rf}_{mr,k}(s) = \frac{\left(1/R_s\right)u^{rf}_{ds,k}(s) + \sigma\tau_s\mathscr{L}\left(i^{rf}_{qs,k}\omega_{\bar{\psi}_{r,k}}\right)}{\sigma\tau_s\tau_r s^2 + \left(\tau_s + \tau_r\right)s + 1}, \tag{21}$$

where $\tau_s$ is the stator time constant that is equal to $\tau_s = L_s/R_s$.

The characteristic polynomial equation of the transfer function given by (21) has always real eigenvalues, which can be derived as follows:

$$\sigma\tau_s\tau_r s^2 + \left(\tau_s + \tau_r\right)s + 1 = 0.0,$$

$$s_{1,2} = \frac{-\left(\tau_s + \tau_r\right)}{2\sigma\tau_s\tau_r} \pm \frac{\sqrt{\left(\tau_s + \tau_r\right)^2 - 4\sigma\tau_s\tau_r}}{2\sigma\tau_s\tau_r}. \tag{22}$$

To get real eigenvalues, the quantity under root square $\sqrt{(\tau_s + \tau_r)^2 - 4\sigma\tau_s\tau_r}$ must be larger than 0.0; thus,

$$\partial = \tau_s^2 + \tau_r^2 + 2\tau_s\tau_r - 4\sigma\tau_s\tau_r > 0.0, \tag{23}$$

and thus (21) can be rewritten by

$$\bar{i}^{rf}_{mr,k}(s) = \frac{1/R_s u^{rf}_{ds,k}(s) + \sigma\tau_s\mathscr{L}\left(i^{rf}_{qs,k}\omega_{\bar{\psi}_{r,k}}\right)}{\left(\left(2\sigma\tau_s\tau_r/\left(\tau_s + \tau_r - \sqrt{\partial}\right)\right)s + 1\right) + \left(\left(2\sigma\tau_s\tau_r/\tau_s + \tau_r + \sqrt{\partial}\right)s + 1\right)}. \tag{24}$$

From (24), it can be realized that the term $\mathscr{L}(i_{qs}\omega_{\bar{\psi}_r})$ can be recognized as a disturbance on which the control system has to be robust.

Now, from (10), (11), and (24), the transfer function that relates to the rotor flux and the input $d$-axis stator voltage component can be expressed by

$$\bar{\psi}^{rf}_{r,k}(s) = \frac{\left(L_m/R_s\right)u^{rf}_{ds,k}(s)}{\left(\left(2\sigma\tau_s\tau_r/\left(\tau_s + \tau_r - \sqrt{\partial}\right)\right)s + 1\right) + \left(\left(2\sigma\tau_s\tau_r/\tau_s + \tau_r + \sqrt{\partial}\right)s + 1\right)} + \frac{\sigma L_m\tau_s\mathscr{L}\left(i^{rf}_{qs,k}\omega_{\bar{\psi}_{r,k}}\right)}{\left(\left(2\sigma\tau_s\tau_r/\left(\tau_s + \tau_r - \sqrt{\partial}\right)\right)s + 1\right) + \left(2\sigma\tau_s\tau_r/\left(\tau_s + \tau_r + \sqrt{\partial}\right)s + 1\right)}. \tag{25}$$

Assuming that, under steady-state operation, the current $\bar{i}^{rf}_{mr,k}$ is constant, from (16), the Laplace transform of $i^{rf}_{qs,k}(s)$ can be obtained and expressed by

$$i^{rf}_{qs,k}(s) = \frac{1/R_s\left[\overbrace{u^{rf}_{qs,k}} - L_s\mathscr{L}\left(i^{rf}_{qs,k}\omega_{\bar{\psi}_{r,k}}\right)\right]}{\sigma\tau_s s + 1}. \tag{26}$$

From (25) and (26), the argument that states that the flux and torque of the FPIM can be regulated using the $d$-$q$ components of stator voltage is verified and approved. Then, via substitution from (12) and (18) into (26), the mathematical model of FPIM can be obtained in the functional diagrams as shown in Figures 3 and 4.

After approving the hypothesis of controlling the torque and flux directly through controlling the $d$-$q$ components of the applied stator voltage, the cost function to be utilized by the proposed DMP VC can be formulated by

$$C^j_k = \left|u^*_{ds,k} - u^{rf}_{ds,k}\right|^j + \left|u^*_{qs,k} - u^{rf}_{qs,k}\right|^j + \left|0.0 - u^{rf}_{xs,k}\right|^j + \left|0.0 - u^{rf}_{ys,k}\right|^j, \tag{27}$$

where $j$ denotes the voltage index.

By checking the terms of the cost function (27), it can be realized that the terms are of the same type and thus there is no need to utilize a weighting factor, which saves the computation time. Moreover, it can be noticed that the controlled variables (the stator voltage components $u^{rf}_{ds,k}$, $u^{rf}_{qs,k}$, $u^{rf}_{xs,k}$, and $u^{rf}_{ys,k}$) can be directly obtained via three different procedures; the first choice is obtained via direct measurements using filters, but this solution is not preferred due to the delay in the system response. The second way to get the voltage components is through calculating the voltages with the help of pulse width modulation (PWM) using the switching states, but this method results in varying and high-switching frequencies, which increases the switching losses. The third

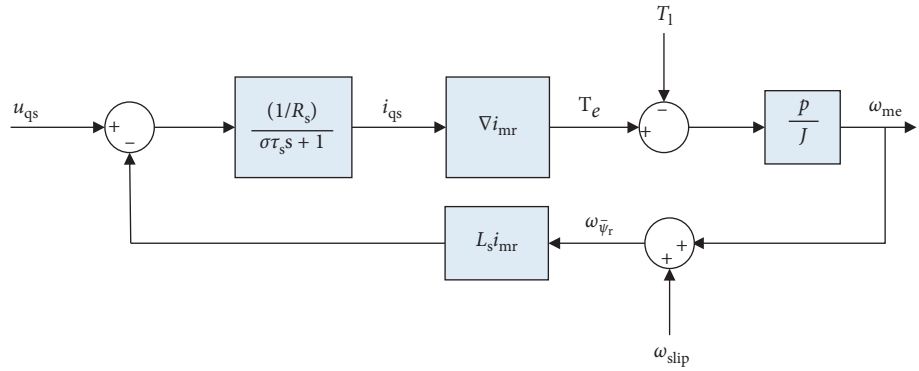


Figure 3: Control of $i_{qs}$ (torque regulation).

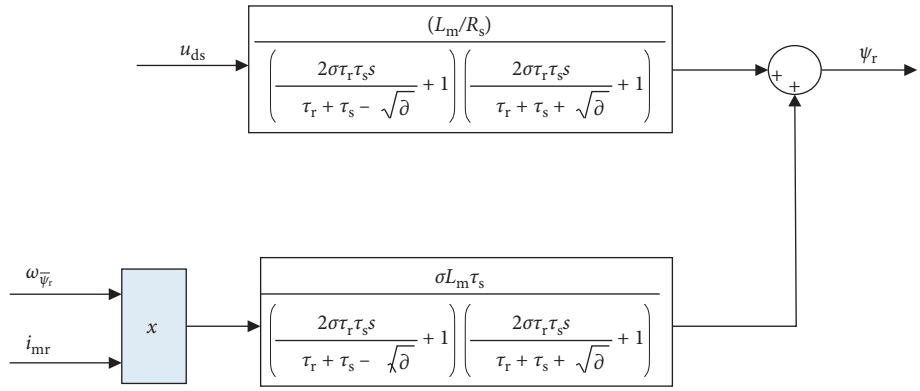


Figure 4: Control of $\psi_r$ (flux regulation).

method is to adopt the finite control set (FCS) principle and calculate the voltages from the switching states ($S_a$, $S_b$, $S_c$, $S_d$, and $S_e$) of the inverter, and this method is adopted here due to its simplicity and reduced computational burden. The calculation of the voltages using the switching states is illustrated by the following formulations:

$$
\begin{aligned}
u_{as,k} &= \frac{U_{dc}}{5}(4S_a - S_b - S_c - S_d - S_e),\\
u_{bs,k} &= \frac{U_{dc}}{5}(4S_b - S_a - S_c - S_d - S_e),\\
u_{cs,k} &= \frac{U_{dc}}{5}(4S_c - S_a - S_b - S_d - S_e),\\
u_{ds,k} &= \frac{U_{dc}}{5}(4S_d - S_a - S_b - S_c - S_e),\\
u_{es,k} &= \frac{U_{dc}}{5}(4S_e - S_a - S_b - S_c - S_d),\\
u^s_{\alpha s,k} &= \sqrt{\frac{2}{5}}\left(u_{as,k} + \cos\left(\frac{2\pi}{5}\right)u_{bs,k} + \cos\left(\frac{4\pi}{5}\right)u_{cs,k} + \cos\left(\frac{4\pi}{5}\right)u_{ds,k} + \cos\left(\frac{2\pi}{5}\right)u_{es,k}\right),\\
u^s_{\beta s,k} &= \sqrt{\frac{2}{5}}\left(\sin\left(\frac{2\pi}{5}\right)u_{bs,k} + \sin\left(\frac{4\pi}{5}\right)u_{cs,k} - \sin\left(\frac{4\pi}{5}\right)u_{ds,k} - \sin\left(\frac{2\pi}{5}\right)u_{es,k}\right),\\
u^s_{xs,k} &= \sqrt{\frac{2}{5}}\left(u_{as,k} + \cos\left(\frac{4\pi}{5}\right)u_{bs,k} + \cos\left(\frac{8\pi}{5}\right)u_{cs,k} + \cos\left(\frac{8\pi}{5}\right)u_{ds,k} + \cos\left(\frac{4\pi}{5}\right)u_{es,k}\right),\\
u^s_{ys,k} &= \sqrt{\frac{2}{5}}\left(\sin\left(\frac{4\pi}{5}\right)u_{bs,k} + \sin\left(\frac{8\pi}{5}\right)u_{cs,k} - \sin\left(\frac{8\pi}{5}\right)u_{ds,k} - \sin\left(\frac{4\pi}{5}\right)u_{es,k}\right),
\end{aligned}
\tag{28}
$$

where the superscript $s$ refers to the quantities defined in stationary frame. Then the feedback $d$-$q$-$x$-$y$ stator voltage components defined in the synchronous reference frame rf can be calculated by

$$\begin{aligned} u_{\mathrm{ds,k}}^{\mathrm{rf}} &= u_{\alpha\mathrm{s,k}}^{\mathrm{s}} \cos\theta_{\overline{\psi}_{\mathrm{r,k}}} + u_{\beta\mathrm{s,k}}^{\mathrm{s}} \sin\theta_{\overline{\psi}_{\mathrm{r,k}}}, \\ u_{\mathrm{qs,k}}^{\mathrm{rf}} &= -u_{\alpha\mathrm{s,k}}^{\mathrm{s}} \sin\theta_{\overline{\psi}_{\mathrm{r,k}}} + u_{\beta\mathrm{s,k}}^{\mathrm{s}} \cos\theta_{\overline{\psi}_{\mathrm{r,k}}}, \\ u_{\mathrm{xs,k}}^{\mathrm{rf}} &= u_{\mathrm{xs,k}}^{\mathrm{s}} \cos\theta_{\overline{\psi}_{\mathrm{r,k}}} + u_{\mathrm{ys,k}}^{\mathrm{s}} \sin\theta_{\overline{\psi}_{\mathrm{r,k}}}, \\ u_{\mathrm{ys,k}}^{\mathrm{rf}} &= -u_{\mathrm{xs,k}}^{\mathrm{s}} \sin\theta_{\overline{\psi}_{\mathrm{r,k}}} + u_{\mathrm{ys,k}}^{\mathrm{s}} \cos\theta_{\overline{\psi}_{\mathrm{r,k}}}. \end{aligned} \tag{29}$$

The reference values of $u_{\mathrm{xs,k}}^{*}$ and $u_{\mathrm{ys,k}}^{*}$ are set to zero to minimize the power losses. The remaining parts of the cost function (27) are the reference values of stator voltage components $u_{\mathrm{ds},k}^{*}$ and $u_{\mathrm{qs},k}^{*}$, which are derived through adopting the deadbeat control principle within the predictive voltage controller. This can be described as follows.

The deadbeat control has the ability to perform a simple and direct treatment of the controlled variables (torque, flux, and current), as it enables the computation of the desired input signal (reference values) ensuring that the actual signals will track definitely the reference signals for each control cycle when applied to a discretized system. For this reason, the deadbeat control is utilized here to generate the references of the $d$-$q$ components of stator voltage vectors, which are then utilized by the cost function besides the actual $d$-$q$ components of stator voltage vectors ($u_{\mathrm{ds,k}}^{*}$ and $u_{\mathrm{qs,k}}^{*}$). The main arguments based upon which the deadbeat control stands can be described as follows.

It is well recognized that the continuous linear system can be described by two relationships as follows:

$$\dot{\overline{x}} = A\overline{x} + B\overline{u} + G\overline{\omega}, \tag{30}$$

$$\overline{y} = C\overline{x}, \tag{31}$$

where, $A$, $B$, $C$, and $G$ are $n * n$ matrices and $C = I$, where $I$ is the identity matrix. In addition, $\overline{\omega}$ denotes the disturbance vector. The relationship in (30) can be discretized and then can be expressed at instant $kT_s$ as follows:

$$\overline{x}(k+1) = A_{\mathrm{d}}\overline{x}_{\mathrm{k}} + B_{\mathrm{d}}\overline{u}_{\mathrm{k}} + G_{\mathrm{d}}\overline{\omega}_{\mathrm{k}}, \tag{32}$$

$$\begin{aligned} A_{\mathrm{d}} &= e^{AT_{\mathrm{s}}} \cong I + AT_{\mathrm{s}}, \\ B_{\mathrm{d}} &= \int_0^{\tau} e^{AT_{\mathrm{s}}} B\mathrm{d}\tau \cong BT_s, \\ G_{\mathrm{d}} &= \int_0^{\tau} e^{AT_{\mathrm{s}}} G\mathrm{d}\tau \cong GT_{\mathrm{s}}. \end{aligned} \tag{33}$$

To maintain the steady-state error at minimum value, the system input vector (the stator voltage $d$-$q$ components) has to be calculated as follows:

$$\overline{u}_{\mathrm{k}} = F\left(\overline{x}_{\mathrm{ref}} - \overline{x}_{\mathrm{k}}\right), \tag{34}$$

where $\overline{x}_{\mathrm{ref}}$ is the reference vector and $F$ is the matrix gain. Then, via substituting (34) into (33) and putting $\overline{x}_{\mathrm{ref}} = \overline{x}_{k+1}$, the input vector that guarantees minimum error can be expressed by

$$\overline{u}_{\mathrm{k}} = B_{\mathrm{d}}^{-1} A_{\mathrm{d}} \left[A_{\mathrm{d}}^{-1}\overline{x}_{\mathrm{ref}} - \overline{x}_{\mathrm{k}} - A_{\mathrm{d}}^{-1} G_{\mathrm{d}}\overline{\omega}_{\mathrm{k}}\right]. \tag{35}$$

The relationships in (34) and (35) can now be applied to the corresponding relationships, which describe the electric dynamics of the FPIM expressed in the $d$-$q$ axes under the RFOC as follows.

The $d$-axis component of the stator voltage under RFOC can be expressed after some mathematical manipulation starting from (2) to (5) by

$$u_{\mathrm{ds,k}}^{\mathrm{rf}} = \left(\frac{R_{\mathrm{s}}}{L_{\mathrm{m}}} - \frac{L_{\mathrm{s}}\tau_{\mathrm{r}}}{L_{\mathrm{m}}}\omega_{\mathrm{sl,k}}\right)\psi_{\mathrm{dr,k}}^{\mathrm{rf}} + \left(\frac{L_{\mathrm{m}}}{L_{\mathrm{r}}} + \frac{L_{\mathrm{t}}}{L_{\mathrm{m}}}\right)\frac{\mathrm{d}\psi_{\mathrm{dr,k}}^{\mathrm{rf}}}{\mathrm{d}t}. \tag{36}$$

Meanwhile, the $q$-axis component of stator voltage can be expressed in the same manner by

$$u_{\mathrm{qs,k}}^{\mathrm{rf}} = R_{\mathrm{s}} i_{\mathrm{qs,k}}^{\mathrm{rf}} + L_{\mathrm{t}}\frac{\mathrm{d}i_{\mathrm{qs,k}}^{\mathrm{rf}}}{\mathrm{d}t} + \left(\frac{L_{\mathrm{m}}}{L_{\mathrm{r}}} + \frac{L_{\mathrm{t}}}{L_{\mathrm{m}}}\right) * \left(\frac{L_{\mathrm{r}} T_{\mathrm{e,k}}}{1.5 L_{\mathrm{m}} i_{\mathrm{qs,k}}^{\mathrm{rf}}}\right)\omega_{\overline{\psi}_{\mathrm{r,k}}}. \tag{37}$$

The relationships in (36) and (37) can be considered as a mirror to the relationships in (25) and (26), which report that the flux and torque can be controlled via controlling the $d$-axis and $q$-axis components of stator voltages, respectively.

According to (34) and (35), and from (36), to achieve the flux control, the predicted value of rotor flux at instant $(k+1)T_{\mathrm{s}}$ must be equal to the reference value so that

$$\psi_{\mathrm{dr,k+1}}^{\mathrm{rf}} = \psi_{\mathrm{r,k}}^{*}. \tag{38}$$

Moreover, the derivative of the rotor flux can be expressed assuming small sampling interval ($T_s$) by

$$\frac{\mathrm{d}\psi_{\mathrm{dr,k}}^{\mathrm{rf}}}{\mathrm{d}t} = \frac{\psi_{\mathrm{dr,k+1}}^{\mathrm{rf}} - \psi_{\mathrm{dr,k}}^{\mathrm{rf}}}{T_{\mathrm{s}}} = \frac{\psi_{\mathrm{r,k}}^{*} - \psi_{\mathrm{dr,k}}^{\mathrm{rf}}}{T_{\mathrm{s}}}. \tag{39}$$

Then, from (39) and by substituting in (36), the reference value of $d$-axis component of stator voltage can be expressed by

$$\widehat{u_{\mathrm{ds,k}}^{*}} = \left(\frac{R_{\mathrm{s}}}{L_{\mathrm{m}}} - \frac{L_{\mathrm{s}}\tau_{\mathrm{r}}}{L_{\mathrm{m}}}\omega_{\mathrm{sl,k}}\right)\psi_{\mathrm{dr,k}}^{\mathrm{rf}} + \left(\frac{L_{\mathrm{m}}}{L_{\mathrm{r}}} + \frac{L_{\mathrm{t}}}{L_{\mathrm{m}}}\right)\widehat{\left(\frac{\psi_{\mathrm{r,k}}^{*} - \psi_{\mathrm{dr,k}}^{\mathrm{rf}}}{T_{\mathrm{s}}}\right)}. \tag{40}$$

In the same manner, based on (34) and (35), and from (37), to realize the torque control, the predicted value of $q$-axis component of stator flux $i_{\mathrm{qs,k+1}}^{\mathrm{rf}}$ must be equal to the reference value $i_{\mathrm{qs,k}}^{*}$, which can be calculated by

$$i_{\mathrm{qs,k}}^{*} = \frac{T_{\mathrm{e,k}}^{*}}{1.5\left(L_{\mathrm{m}}/L_{\mathrm{r}}\right)\psi_{\mathrm{r,k}}^{*}}, \tag{41}$$

and, via assuming the sampling interval to be with small value, the current derivative $\mathrm{d}i_{\mathrm{qs,k}}^{\mathrm{rf}}/\mathrm{d}t$ can be expressed by

$$\frac{\mathrm{d}i_{\mathrm{qs,k}}^{\mathrm{rf}}}{\mathrm{d}t} = \frac{i_{\mathrm{qs,k+1}}^{\mathrm{rf}} - i_{\mathrm{qs,k}}^{\mathrm{rf}}}{T_{\mathrm{s}}} = \frac{i_{\mathrm{qs,k}}^{*} - i_{\mathrm{qs,k}}^{rf}}{T_{\mathrm{s}}}. \tag{42}$$

Then, from (42) and by substituting into (37), the $q$-axis voltage reference is calculated by

$$\widehat{u^*_{\mathrm{qs,k}}} = R_{\mathrm{s}} i^{\mathrm{rf}}_{\mathrm{qs,k}} + L_{\mathrm{t}} \widehat{\left(\frac{i^*_{\mathrm{qs,k}} - i^{\mathrm{rf}}_{\mathrm{qs,k}}}{T_{\mathrm{s}}}\right)} + \left(\frac{L_{\mathrm{m}}}{L_{\mathrm{r}}} + \frac{L_{\mathrm{t}}}{L_{\mathrm{m}}}\right) * \left(\frac{L_{\mathrm{r}} T_{\mathrm{e,k}}}{1.5 L_{\mathrm{m}} i^{\mathrm{rf}}_{\mathrm{qs,k}}}\right) \omega_{\overline{\psi}_{\mathrm{r,k}}}. \tag{43}$$

Till now, the reference voltage components ($u^*_{\mathrm{ds,k}}$ and $u^*_{\mathrm{qs,k}}$) to be used by cost function (27) are obtainable, and then the control system can start the computation.

To investigate more about the selection mechanism of optimal voltage vector using the proposed cost function of (27) which based operation depends on achieving the minimum error between the actual applied voltage vectors and the reference voltage vectors, the voltage vectors displacement and their corresponding switching states are illustrated in Figure 5. It can be realized that, for a given reference voltage vector $\overline{u}_s^*$ located in sector 9, there will be seven possible voltage vectors which can achieve the control target (vector 19, vector 17, vector 1, vector 27, vector 18, vector 21, and vector 31 or 32). However, the optimal one that will be selected using the cost function of (27) is the vector that achieves minimum error (distance between the actual vector and reference vector $\overline{u}_s^*$), which is here vector 17 that makes an error of $\overline{u}_{\mathrm{e17}}$. This process is performed without using any estimated quantities (in comparison with the MP DTC approach), which saves the computation time of the controller and reduces the switching losses of the inverter.

## 4. The Proposed Back-Stepping Observer

*4.1. Mathematical Model of the Back-Stepping Observer.* The minimization of the error between the estimated and measured stator current values is the base principle upon which the back-stepping observer is designed. It is assumed that the components of the stator current are the outputs of the system which can be expressed by

$$\begin{cases} y_1 = x_1, \\ y_2 = x_2. \end{cases} \tag{44}$$

Moreover, the model of the back-stepping observer is given by

$$\begin{cases} \dot{\hat{x}}_1 = -\widehat{A}\hat{x}_1 + K.\widehat{A}_{\mathrm{r}}\hat{x}_3 + K.\widehat{\omega}_{\mathrm{me}}\hat{x}_4 + B.u_{\alpha\mathrm{s}} + V_\alpha, \\ \dot{\hat{x}}_2 = -\widehat{A}\hat{x}_2 + K.\widehat{A}_{\mathrm{r}}\hat{x}_4 - K.\widehat{\omega}_{\mathrm{me}}\hat{x}_3 + B.u_{\beta\mathrm{s}} + V_\beta, \\ \dot{\hat{x}}_3 = L_{\mathrm{m}}\widehat{A}_{\mathrm{r}}\hat{x}_1 - \widehat{A}_r\hat{x}_3 - \widehat{\omega}_{\mathrm{me}}\hat{x}_4, \\ \dot{\hat{x}}_4 = L_{\mathrm{m}}\widehat{A}_{\mathrm{r}}\hat{x}_2 - \widehat{A}_{\mathrm{r}}\hat{x}_4 + \widehat{\omega}_{\mathrm{me}}\hat{x}_3, \end{cases} \tag{45}$$

where

$$\begin{aligned} \left[\, x_1 \;\; x_2 \;\; x_3 \;\; x_4 \,\right]^T &= \left[\, i_{\alpha\mathrm{s}} \;\; i_{\beta\mathrm{s}} \;\; \psi_{\alpha\mathrm{r}} \;\; \psi_{\beta\mathrm{r}} \,\right]^T, \\ \widehat{A}_{\mathrm{r}} &= A_{\mathrm{r}} + \Delta A_{\mathrm{r}} = \frac{R_{\mathrm{r}}}{L_{\mathrm{r}}} + \frac{\Delta R_{\mathrm{r}}}{L_{\mathrm{r}}}, \\ \widehat{R}_\vartheta &= R_{\mathrm{s}} + L_{\mathrm{m}} \cdot \mu \Delta \widehat{A}_{\mathrm{r}}, \\ \widehat{A} &= \frac{\widehat{R}_\vartheta}{\sigma L_{\mathrm{s}}} = \frac{R_\vartheta}{\sigma L_{\mathrm{s}}} + \frac{L_{\mathrm{m}} \cdot \mu \cdot \Delta a_r}{\sigma L_{\mathrm{s}}} = A + \Delta A, \\ K &= \frac{L_{\mathrm{m}}}{\sigma L_{\mathrm{s}} L_{\mathrm{r}}}, \\ \mu &= \frac{L_{\mathrm{m}}}{L_{\mathrm{r}}}, \end{aligned} \tag{46}$$

where $\hat{x}_i$ is the estimate of $x_i$ for $i \in \{1, 2, 3, 4\}$.

$V_\alpha$ and $V_\beta$ represent the vector components that are built by the back-stepping strategy. In addition, all the parameters of the five-phase induction motor are considered to be known except the rotor resistance. The rotor resistance $R_{\mathrm{r}}$ is considered as an uncertain parameter of nominal rotor resistance $R_{\mathrm{rn}}$.

*4.2. Dynamic Model of the Estimation Errors.* The equations of state errors are formulated as follows:

$$z_i = \begin{bmatrix} z_{y1} = z_{x_1} \\ z_{y2} = z_{x_2} \end{bmatrix} = \begin{bmatrix} x_1 - \hat{x}_1 \\ x_2 - \hat{x}_2 \end{bmatrix}, \tag{47}$$

$$z_\psi = \begin{bmatrix} z_{x_3} \\ z_{x_4} \end{bmatrix} = \begin{bmatrix} x_3 - \hat{x}_3 \\ x_4 - \hat{x}_4 \end{bmatrix}, \tag{48}$$

where $z_i$ and $z_\psi$ represent the observation errors of the stator current and the rotor flux, respectively.

Using (44), (47), and (48), the dynamic model of prediction errors is given by

$$\begin{cases} \dot{z}_{x_1} = K\left(\left(A_r z_{x_3} + \omega_{\mathrm{me}} z_{x_4}\right) + \Delta\omega_{\mathrm{me}}\hat{x}_4 + \Delta A_{\mathrm{r}}\left(L_{\mathrm{m}}x_1 - \hat{x}_3\right)\right) - V_\alpha, \\ \dot{z}_{x_2} = K\left(\left(A_{\mathrm{r}} z_{x_4} - \omega_{\mathrm{me}} z_{x_3}\right) - \Delta\omega_{\mathrm{me}}\hat{x}_3 + \Delta A_{\mathrm{r}}\left(L_{\mathrm{m}}x_2 - \hat{x}_4\right)\right) - V_\beta, \\ \dot{z}_{x_3} = -\left(A_{\mathrm{r}} z_{x_3} + \omega_{\mathrm{me}} z_{x_4}\right) - \Delta\omega_{\mathrm{me}}\hat{x}_4 + \Delta A_{\mathrm{r}}\left(L_{\mathrm{m}}x_1 - \hat{x}_3\right), \\ \dot{z}_{x_4} = \left(-A_{\mathrm{r}} z_{x_4} + \omega_{\mathrm{me}} z_{x_3}\right) + \Delta\omega_{\mathrm{me}}\hat{x}_3 + \Delta A_{\mathrm{r}}\left(L_{\mathrm{m}}x_2 - \hat{x}_4\right), \end{cases} \tag{49}$$

where the speed error is given by $\Delta\omega_{\mathrm{me}} = \omega_{\mathrm{me}} - \widehat{\omega}_{\mathrm{me}}$. In order to solve the problem of tracking and regulating the speed and rotor flux and to overcome the difficulties that arise due to the unavailability of direct measurement of one of the state vector variables [30, 31], a nonlinear back-stepping observer is proposed.

| |
|---|
| 1: 00001 |
| 2: 00010 |
| 3: 00011 |
| 4: 00100 |
| 5: 00101 |
| 6: 00110 |
| 7: 00111 |
| 8: 01000 |
| 9: 01001 |
| 10: 01010 |
| 11: 01011 |
| 12: 01100 |
| 13: 01101 |
| 14: 01110 |
| 15: 01111 |
| 16: 10000 |
| 17: 10001 |
| 18: 10010 |
| 19: 10011 |
| 20: 10100 |
| 21: 10101 |
| 22: 10110 |
| 23: 10111 |
| 24: 11000 |
| 25: 11001 |
| 26: 11010 |
| 27: 11011 |
| 28: 11100 |
| 29: 11101 |
| 30: 11110 |
| 31: 11111 |
| 32: 00000 |

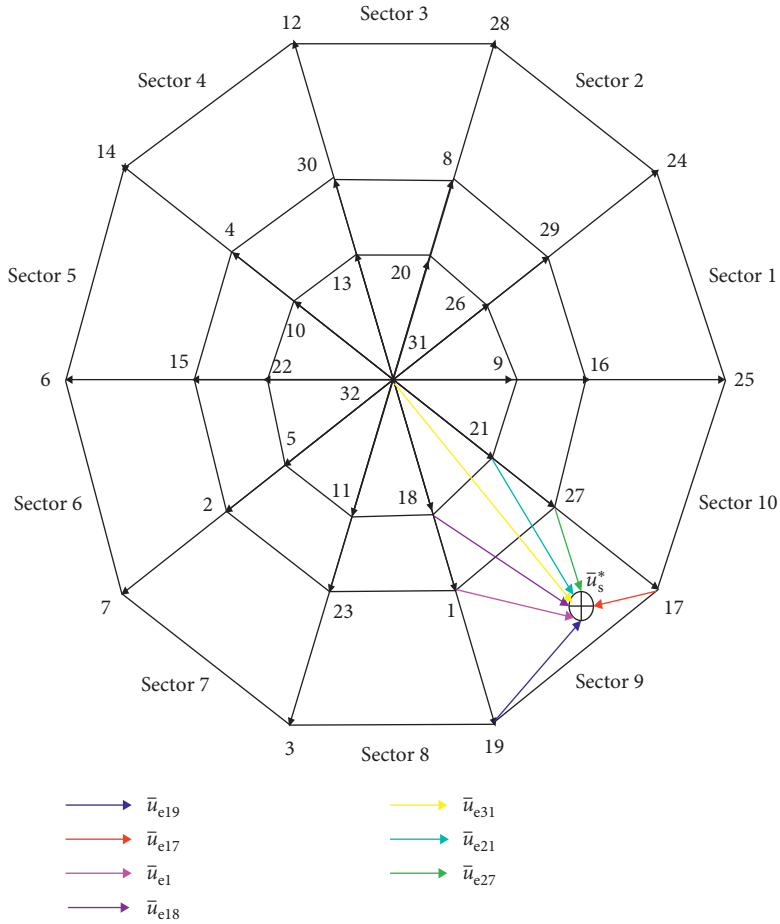


FIGURE 5: Optimal voltage vector ($\bar{u}_s^*$) selection mechanism.

*4.3. Synthesis of the Nonlinear Back-Stepping Observer.* The synthesis of the nonlinear back-stepping observer takes place in two stages.

*Step 1.* The first step for the synthesis of the nonlinear back-stepping observer is to design a stability controller for the integral of the prediction errors $z_{y_1}$ and $z_{y_2}$ using the virtual command variables $z_{x_1}$ and $z_{x_2}$ with stabilization functions $(y_{c\alpha}, y_{c\beta})$, where $y_{c\alpha}$ and $y_{c\beta}$ are the reference trajectories for the virtual variables. Then, the integral of the prediction errors of the currents $z_{x_\alpha}$ and $z_{x_\beta}$ can be expressed by

$$\begin{cases} \dot{z}_{x_\alpha} = z_{x_1}, \\ \dot{z}_{x_\beta} = z_{x_2}. \end{cases} \tag{50}$$

Moreover, the prosecution errors $Z_\alpha$ and $Z_\beta$ for the integral of the prediction errors $z_{y_1}$ and $z_{y_2}$ are defined by

$$\begin{cases} Z_\alpha = z_{y_1} - y_{c\alpha}, \\ Z_\beta = z_{y_2} - y_{c\beta}. \end{cases} \tag{51}$$

Knowing that the dynamics of the observer depend on the exponential convergence, the variations of the reference trajectories for the virtual variables can be imposed using the following expressions:

$$\begin{cases} y_{c_1} = -\lambda_1 z_{x_\alpha}, \\ y_{c_2} = -\lambda_2 z_{x_\beta}. \end{cases} \tag{52}$$

*Step 2.* In this step, by substituting (52) into (51), the errors $Z_\alpha$ and $Z_\beta$ can be expressed by

$$\begin{cases} Z_\alpha = z_{y_1} + \lambda_1 z_{x_\alpha}, \\ Z_\beta = z_{y_2} + \lambda_2 z_{x_\beta}. \end{cases} \tag{53}$$

Using (48), (50), and (53), the control inputs $V_\alpha$ and $V_\beta$ can be formulated by

$$\begin{cases} V_\alpha = K\left(A_r z_{x_3} + \omega_{me} z_{x_4} + \Delta\omega_{me}\hat{x}_4\right) + \lambda_1 z_{x_1} + \lambda_2 Z_\alpha + z_{x_\alpha}, \\ V_\beta = K\left(A_r z_{x_4} - \omega_{me} z_{x_3} - \Delta\omega_{me}\hat{x}_3\right) + \lambda_1 z_{x_2} + \lambda_2 Z_\beta + z_{x_\beta}. \end{cases} \tag{54}$$

By substituting (54) into (53), this results in

$$\begin{cases} \dot{Z}_\alpha = -Az_{x_1} + K\left(\left(A_r z_{x_3} + \omega_{me} z_{x_4}\right) + \Delta\omega_{me}\widehat{x}_4 + \Delta A_r\left(L_m x_1 - \widehat{x}_3\right)\right) - V_\alpha + \lambda_1 z_{x_1}, \\ \dot{Z}_\beta = -Az_{x_2} + K\left(\left(A_r z_{x_4} - \omega_{me} z_{x_3}\right) - \Delta\omega_{me}\widehat{x}_3 + \Delta A_r\left(L_m x_2 - \widehat{x}_4\right)\right) - V_\beta + \lambda_1 z_{x_2}, \end{cases} \tag{55}$$

where $\lambda_1$ and $\lambda_2$ are positive constants that determine the dynamics of the closed-loop system.

*4.4. Rotor Speed and Rotor Resistance Estimation.* The backstepping mechanism has been formulated based on Lyapunov's second method, which combines the choice of the system function with those of the control laws. This allows, in addition to the task for which the controller is designed (tracking and/or regulation), ensuring the overall stability of the compensated system. However, it is characterized by its sensitivity to the variation of the rotor time constant. The latter also depends on the temperature variations as well as the saturation of the machine. The variation of the rotor time constant directly affects the tuning performance and the efficiency of the induction motor. Thus, due to these reasons, it is mandatory to apply a mechanism for the online estimation and adaptation of the rotor resistance. For the design of the observer and the online adaptation mechanism of the rotor resistance, a candidate Lyapunov function must be defined, which includes all the tracking errors increased by the errors of the speed and rotor resistance, and this can be formulated using the following relationship:

$$V_L = \frac{1}{2}\left(z_{x\alpha}^2 + z_{x\beta}^2 + Z_\alpha^2 + Z_\beta^2 + z_{x3}^2 + z_{x4}^2 + \frac{\Delta\omega_{me}^2}{\varepsilon} + \frac{\Delta R_r^2}{\Sigma}\right), \tag{56}$$

where $\varepsilon$ and $\Sigma$ are positive constants.

Using (49), (53), and (55), the derivative of (56) gives

$$\begin{aligned} \dot{V}_L = {} & -\lambda_1 z_{x\alpha}^2 - \lambda_1 z_{x\beta}^2 - \lambda_2 Z_\alpha^2 - \lambda_2 Z_\beta^2 - \frac{\widehat{R}_r}{L_r} z_{x3}^2 - \frac{\widehat{R}_r}{L_r} z_{x3}^2 \\ & + \Delta R_r\left(\frac{K}{L_r} Z_\alpha x_3 - K\mu Z_\alpha x_1 + \frac{K}{L_r} Z_\beta x_4 - K\mu Z_\beta x_2 - \frac{x_3 z_{x3}}{L_r} + \mu x_1 z_{x3} - \frac{x_4 z_{x4}}{L_r} + \mu x_2 z_{x4} + \frac{1}{\Sigma}\frac{d\Delta R_r}{dt}\right) \\ & + \Delta\omega_{me}\left(\text{P.K}\left(\widehat{\psi}_{\beta r} - \widehat{\psi}_{\alpha r}\right) + \frac{1}{\varepsilon}\frac{d\Delta\omega_{me}}{dt}\right). \end{aligned} \tag{57}$$

The candidate function of Lyapunov $V_L$ is positive-definite. For obtaining a negative derivative of $V_L$, the following conditions must be achieved:

$$\begin{aligned} \Delta R_r\left(\frac{K}{L_r} Z_\alpha x_3 - K\mu Z_\alpha x_1 + \frac{K}{L_r} Z_\beta x_4 - K\mu Z_\beta x_2 - \frac{x_3 z_{x3}}{L_r} + \mu x_1 z_{x3} - \frac{x_4 z_{x4}}{L_r} + \mu x_2 z_{x4} + \frac{1}{\Sigma}\frac{d\Delta R_r}{dt}\right) = 0, \\ \Delta\omega_{me}\left(\text{P.K}\left(\widehat{\psi}_{\beta r} - \widehat{\psi}_{\alpha r}\right) + \frac{1}{\varepsilon}\frac{d\Delta\omega_{me}}{dt}\right) = 0. \end{aligned} \tag{58}$$

This leads to expressing the adaptation mechanisms of the rotor resistance and rotor speed as follows:

$$\frac{d\Delta R_r}{dt} = \Sigma\left(K\mu Z_\beta x_2 + \frac{x_3 z_{x_3}}{L_r} - \mu x_1 z_{x_3} + \frac{x_4 z_{x_4}}{L_r} - \mu x_2 z_{x_4} - \frac{K}{L_r} Z_\alpha x_3 + K\mu Z_\alpha x_1 - \frac{K}{L_r} Z_\beta x_4\right). \tag{59}$$

Via applying the adaptation mechanism and considering that the speed of rotation is an unknown parameter, the rotor speed can be estimated using the Lyapunov theory as follows:

$$\frac{d\Delta\omega_{me}}{dt} = \varepsilon \cdot p \cdot K\left(\widehat{\psi}_{\beta r} - \widehat{\psi}_{\alpha r}\right), \tag{60}$$

where $p$ is pole pair number.

The observer parameters are chosen as follows:

$$\begin{aligned} \varepsilon &= 0.01, \\ \Sigma &= 0.01. \end{aligned} \tag{61}$$

In order to have a focused view of the complete back-stepping observer, Figure 6 illustrates the layout of the proposed observer, which takes the $\alpha$-$\beta$-$x$-$y$ ($u_{\alpha s}, u_{\beta s}, u_{xs}, u_{ys}$) components of measured stator voltage and the $\alpha$-$\beta$-$x$-$y$ ($x_1, x_2, x_5, x_6$) components of measured stator current in addition to the $\alpha$-$\beta$ components of the rotor flux ($x_3, x_4$) as inputs and provides the estimated stator current components ($x_{1,ob}, x_{2,ob}, x_{5,ob}, x_{6,ob}$), the estimated rotor speed ($\omega_{me,ob}$), and the estimated rotor resistance ($R_{r,ob}$) as outputs.

## 5. Complete System Layout

The proposed direct model predictive voltage control (DMP VC) starts its operation with measuring the stator voltage and stator current, and then the measured signals are sampled using the sampling/holding. After that, the sampled signals are used to feed the input of the proposed back-stepping observer, which estimates the stator current, rotor flux, rotor resistance, and the speed. The estimated speed $\widehat{\omega}_{me,k}$ is then used for closing the speed loop to get the reference torque $T^*_{e,k}$ by which the reference $q$-axis component of stator current $i^*_{qs,k}$ is calculated. Meanwhile, the reference of rotor flux $|\psi_r|^*_k$ is applied directly as shown in Figure 7, which shows the control system layout.

The estimated stator current, the estimated rotor resistance, the sampled stator voltage, and the estimated speed are then utilized to predict the stator current and rotor flux at instant $(k+1)T_s$. Then, the predicted values of $\widetilde{i}_{qs,k+1}$ and $\widetilde{\psi}_{dr,k+1}$ besides the references $i^*_{qs,k}$ and $|\psi_r|^*_k$ are used to calculate the $d$-$q$ reference components of stator voltage ($u^*_{ds,k}$ and $u^*_{qs,k}$) utilizing the relationships in (40) and (43).

The reference $d$-$q$ components of stator voltage are then used by the cost function of (27) to determine the optimal voltage vector to be applied to the FPIM's stator terminals. It is worth noticing that the feedback voltage signals ($u_{ds,k}$, $u_{qs,k}$, $u_{xs,k}$, and $u_{ys,k}$) to be used by the cost function (27) are calculated using the switching states of the inverter and applied to the cost function with the help of a memory block. From Figure 7, it can be realized that the proposed DMP VC has a simple configuration, which does not require extra computation for estimating the variables such as torque and flux needed to be predicted in the conventional MP DTC. Thus, it is expected that the proposed DMP VC will have lower switching losses compared with the other two techniques.

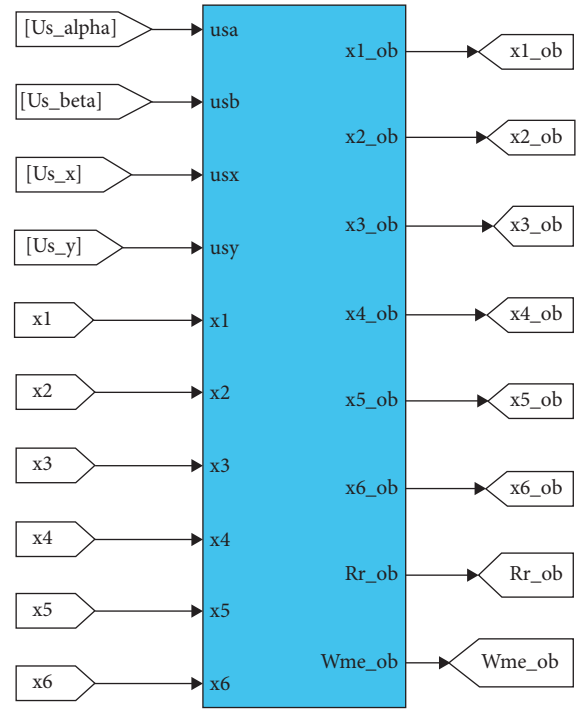


Figure 6: Inputs and outputs of the proposed back-stepping observer.

## 6. Test Results

To verify the operation dynamics of the described sensorless DMP VC algorithm with the FPIM drive, comprehensive tests are performed for two ranges of speed operation, the high speed (1400 rpm) and low speed (30 rpm), while changing the rotor resistance value (this is to test the system robustness to uncertainties). The parameters and control coefficients of the FPIM drive are presented in Table 1.

### 6.1. High Speed Operation

*6.1.1. Performance of FPIM Drive under MP DTC (High Speed).* The performance of FPIM drive for high speed operation and when adopting the MP DTC approach is tested in this section. The FPIM drive is commanded to rotate at a speed of 1400 rpm. A full-load torque is applied at time $t = 1.5$ s and removed at time $t = 3$ s, respectively. The rotor flux reference value is set to its nominal value. The effectiveness of the proposed sensorless back-stepping observer can be synthesized through the obtained results. For example, in Figure 8, the estimated speed is tracking the actual speed with high precision. Furthermore, from Figures 9–12, it can be noticed that the estimated stator current ($\alpha$-$\beta$) components and rotor flux ($\alpha$-$\beta$) components are tracking their actual values with minimum deviations.

The validity of the proposed back-stepping observer can be also checked and verified from Figure 13, which shows that the estimated rotor resistance is definitely tracking the resistance variation. Figures 14 and 15 illustrate the estimated rotor position and the estimation error, respectively.

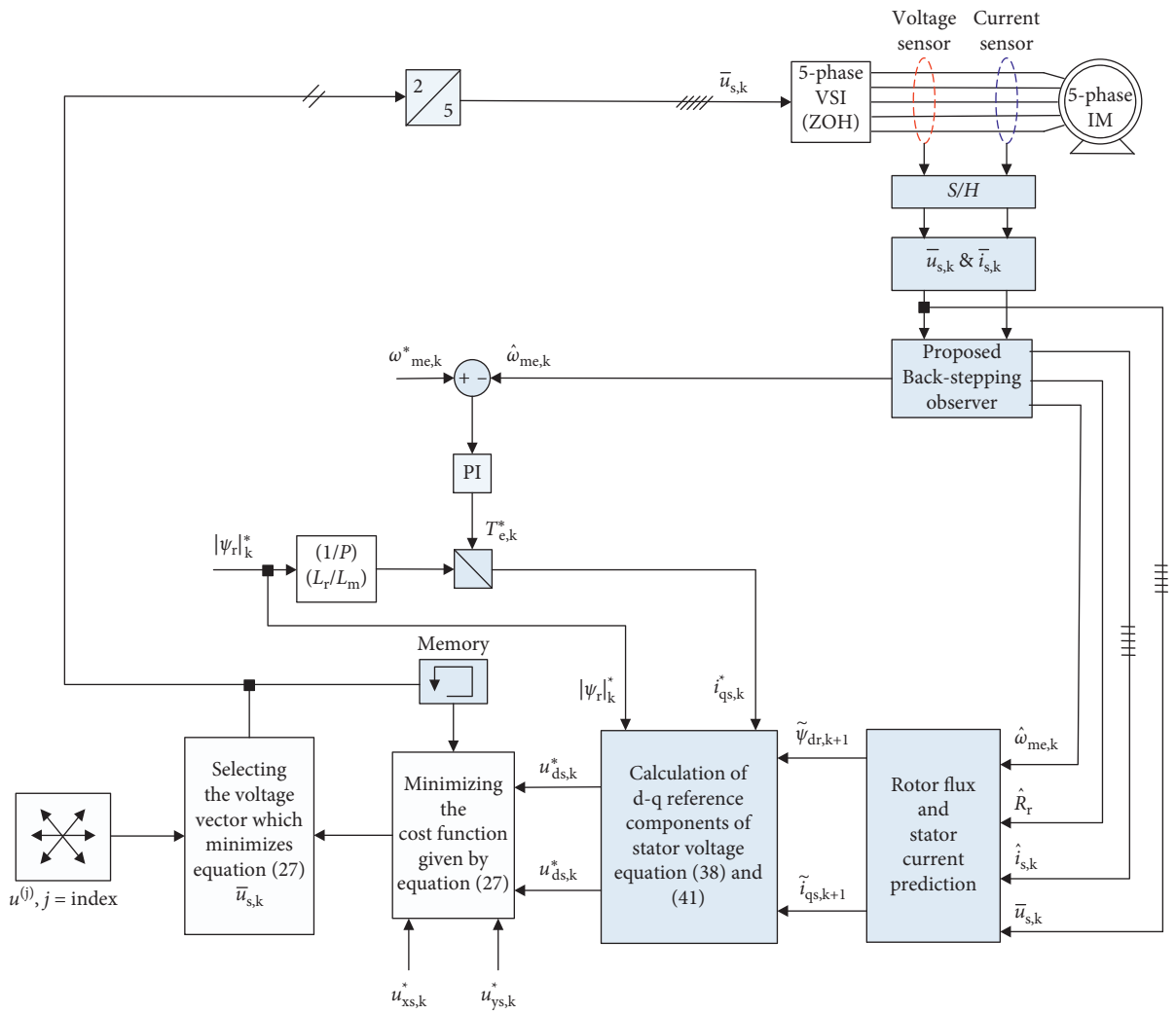


Figure 7: Complete system layout for the proposed DMP VC approach for FPIM drive.

Table 1: Parameters of FPIM.

| Parameters | Value |
|---|---|
| Rated torque | 8 nm |
| $R_s$ | 10 Ω |
| $R_r$ | 6.3 Ω |
| $L_s$ | 460 mH |
| $L_r$ | 460 mH |
| $p$ (pole pairs) | 2 |
| $L_m$ | 420 mH |
| $\Psi_{rn}$ (nominal rotor flux) | 0.86 Vs |
| $U_{dc}$ (dc link voltage) | 400 V |
| $J_m$ | 0.03 kg·m$^2$ |
| $B_m$ | 0.008 Nm·rad·s$^{-1}$ |
| $T_s$ (sampling time) | 100 $\mu$s |

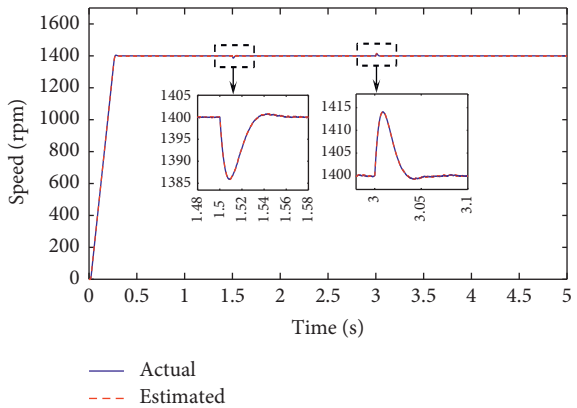


Figure 8: Rotor speed under MP DTC (rpm).

From these two figures, it can be confirmed that the observer has managed to achieve its goal via realizing minimum rotor position estimation error. Figures 16 and 17 show a sample of phase "a" stator current and its FFT spectrum analysis, respectively. From these two figures, it can be noticed that there is a remarkable ripples content in the current waveform under the MP DTC. This fact can be also observed from the stator flux loci shown in Figure 18.

A detailed view about the control action taken under the MP DTC is illustrated through Figures 19–21, which show the stator flux deviation (ripples), the torque deviation

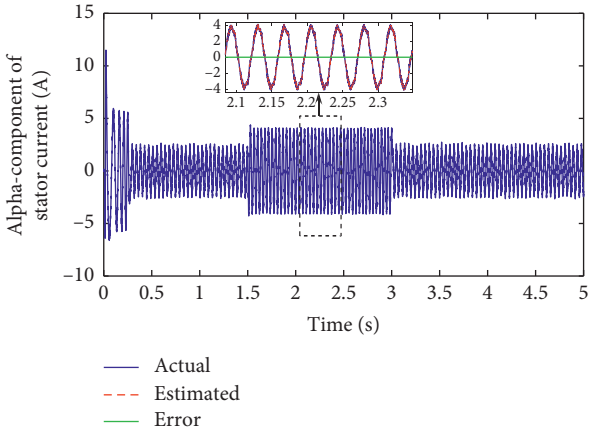


Figure 9: $\alpha$-component of current for MP DTC (A).

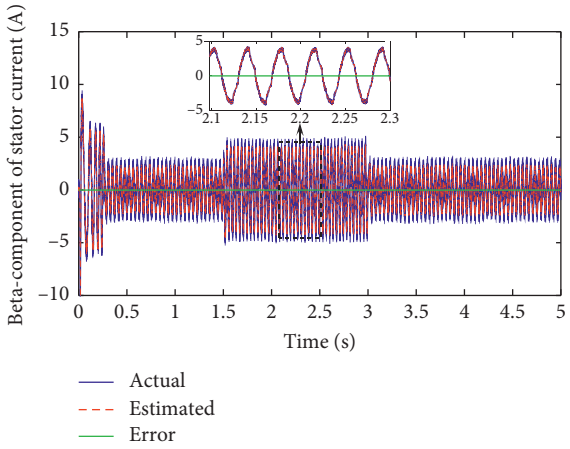


Figure 10: $\beta$-component of current for MP DTC (A).

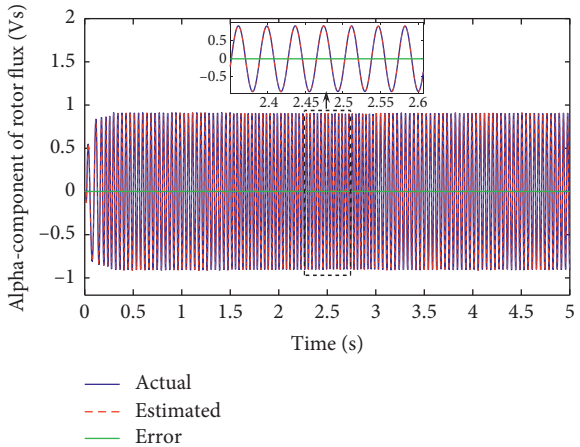


Figure 11: $\alpha$-component of flux for MP DTC (Vs).

(ripples), and the absolute error. From these figures, it can be concluded that, under the MP DTC, the ripples content is noticeable and comparable with the other two control approaches as will be illustrated later. The absolute error is exhibiting a value of 0.21, while the FFT analysis for the stator current presents a total harmonic distortion (THD) of 5.15% of the fundamental.

The $d$-$q$ components of the applied stator voltage are shown in Figure 22, which shows the variation of the $q$-axis component of stator voltage with respect to the change in the applied torque, while the $d$-axis components follow the flux dynamics.

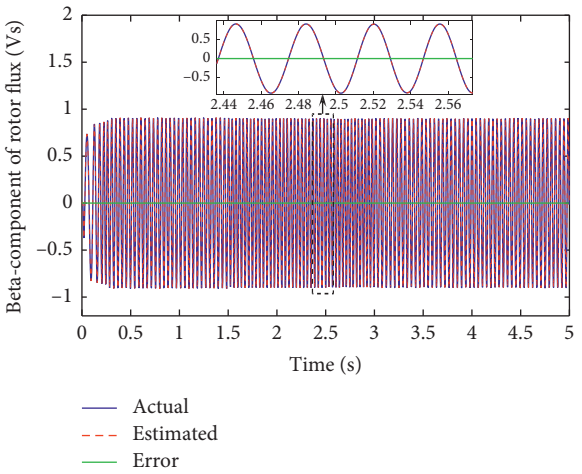


Figure 12: $\beta$-component of rotor for MP DTC (Vs).

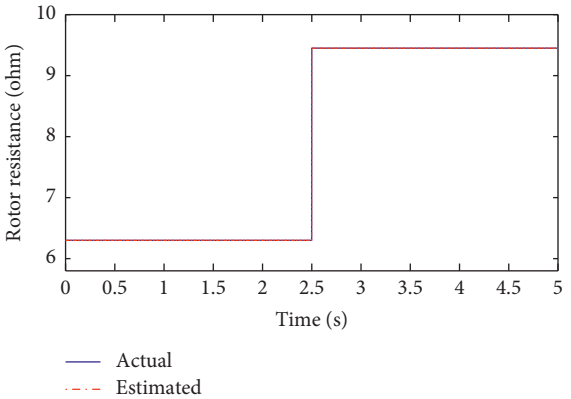


Figure 13: $R_r$ resistance variation under MP DTC ($\Omega$).

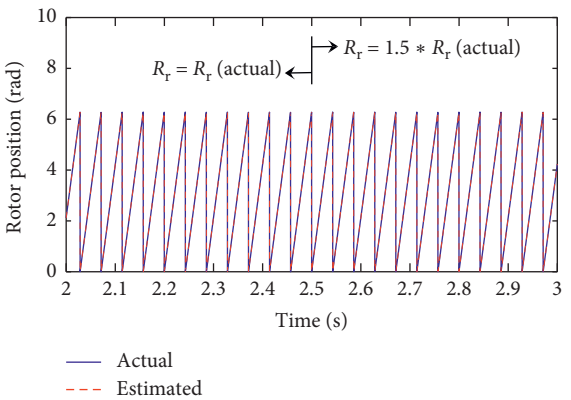


Figure 14: Rotor position under MP DTC (rad).

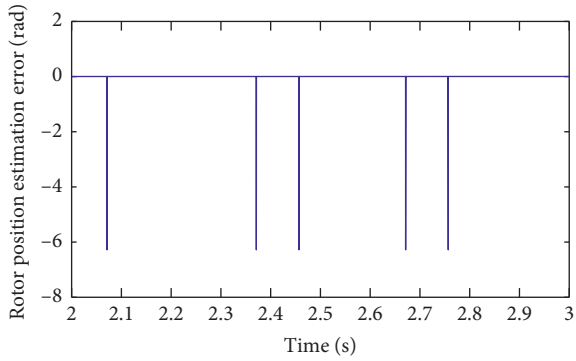


Figure 15: Rotor position error under MP DTC (rad).

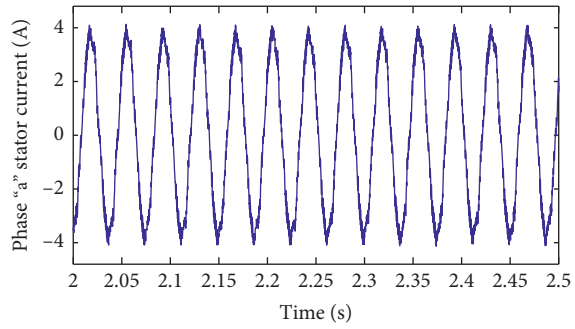


Figure 16: Phase "a" stator current under MP DTC (A).

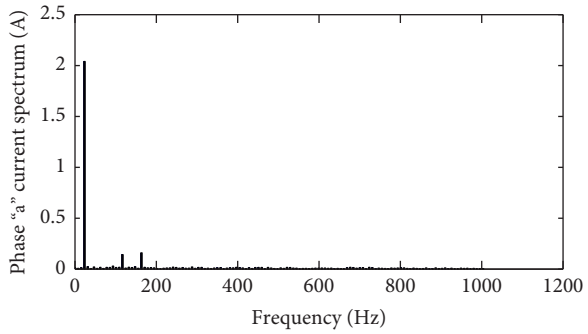


Figure 17: Phase "a" stator current spectrum.

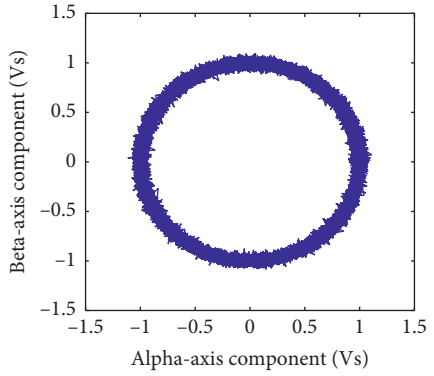


(a)

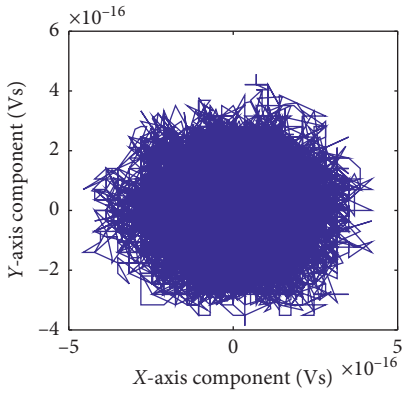


(b)

Figure 18: Stator flux loci under MP DTC.

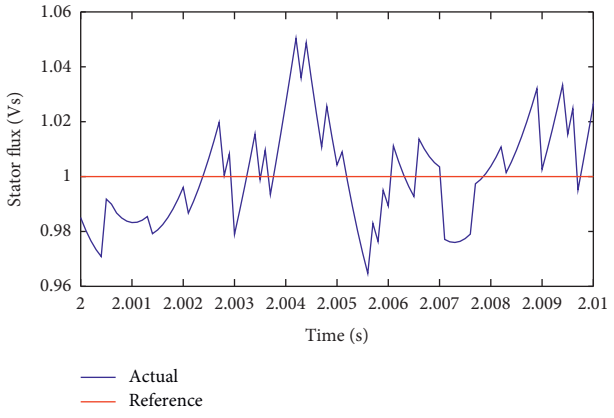


Figure 19: Stator flux ripples under MP DTC (Vs).

*6.1.2. Performance of FPIM Drive under the sProposed DMP VC (High Speed).* In this test, the effectiveness of the proposed sensorless DMP VC is investigated. The test is carried out for the same conditions of the previous test (with MP DTC). The superiority of the proposed DMP VC over the MP DTC control procedure can be synthesized from the obtained results. For example, Figures 23 and 24 show the phase "a" current and its FFT spectrum, respectively. From these two figures, it can be noticed that the stator current exhibits less ripples content compared with the MP DTC values. The THD of the stator current is now 0.53% of the fundamental.

Moreover, the effectiveness of the proposed back-stepping observer is verified with the DMP VC, and this can be observed through Figures 25–29, which illustrate a high precision in estimating the rotor speed, the stator flux ($\alpha$-$\beta$) components, and rotor flux ($\alpha$-$\beta$) components with minimum error.

Figures 30–32 report the validity of the back-stepping observer in estimating the rotor resistance and rotor position with minimum error.

The reduced ripples values with the DMP VC can be also observed through Figures 33–36, which show the stator flux loci, the stator flux fluctuation, the torque oscillation, and the absolute average error, which here is exhibiting a value of 0.051. Moreover, the $d$-$q$ components

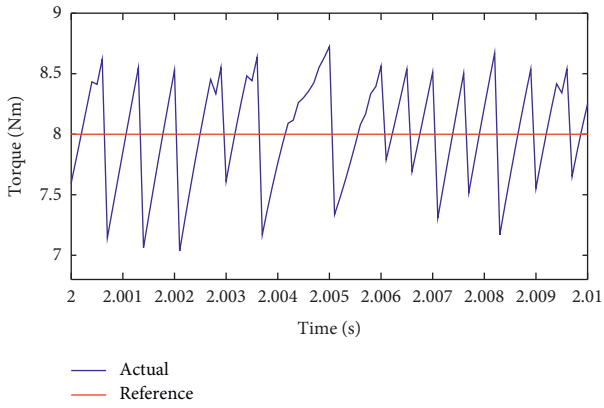


Figure 20: Torque ripples under MP DTC (Nm).

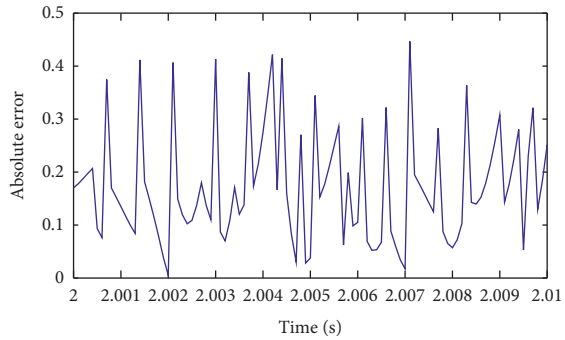


Figure 21: Absolute error under MP DTC.

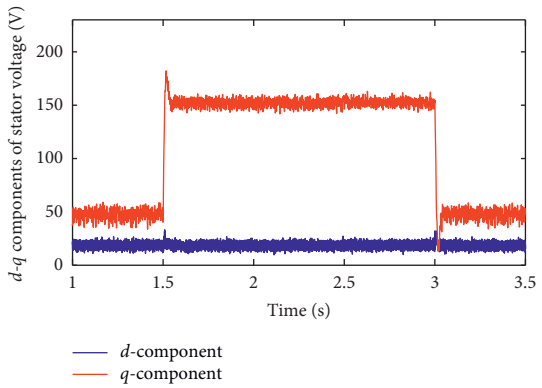


Figure 22: *d-q* components of stator voltage under MP DTC (V).

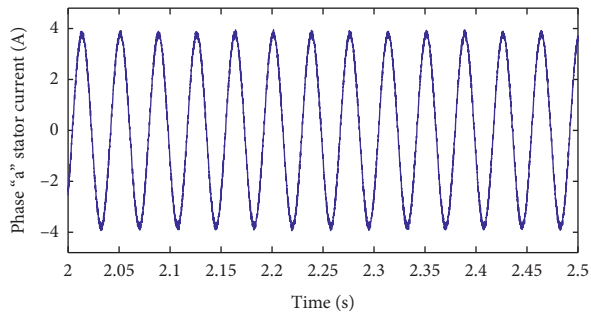


Figure 23: Phase "a" stator current under DMP VC (A).

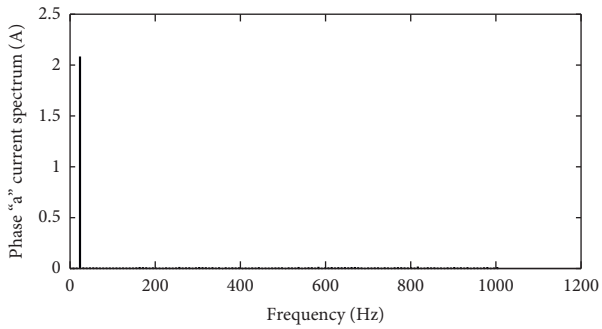


Figure 24: Phase "a" stator current spectrum.

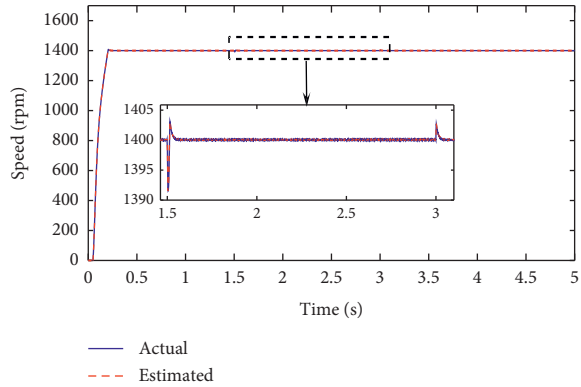


Figure 25: Rotor speed under DMP VC (rpm).

of stator voltage shown in Figure 37 are accompanied by low ripples compared with their values under the MP DTC.

The reduced ripples content when applying the DMP VC can be also noticed from the comparison made in terms of the torque, stator flux, and stator flux loci. This comparison is shown through Figure 38, which shows that the developed torque under the proposed DMP VC is presenting less fluctuation. Figure 39 shows that the stator flux under the proposed DMP VC has lower ripples content, while the comparison in terms of the flux loci is shown in Figure 40, which reconfirms the priority of the proposed DMP VC in reducing the ripples in a better manner than the other two techniques. In addition, the absolute error profiles for the two control methods are shown in Figure 41, clarifying that the DMP VC results in lower error than the MP DTC.

### 6.2. Low Speed Operation

*6.2.1. Performance of FPIM Drive under MP DTC (Low Speed).* The performance of the FPIM drive when implementing the MP DTC approach is performed to check the validity of the proposed back-stepping observer at low speed operation.

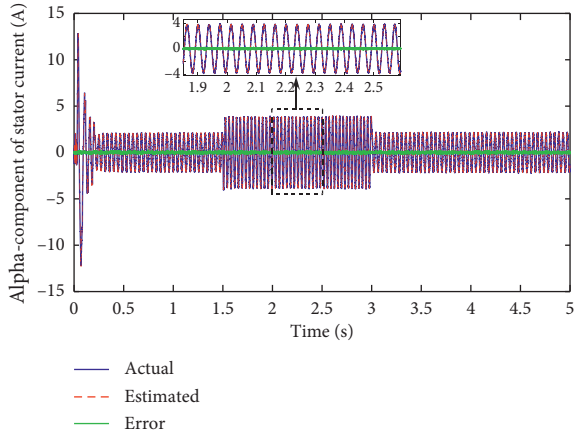


Figure 26: $\alpha$-Component of current for DMP VC (A).

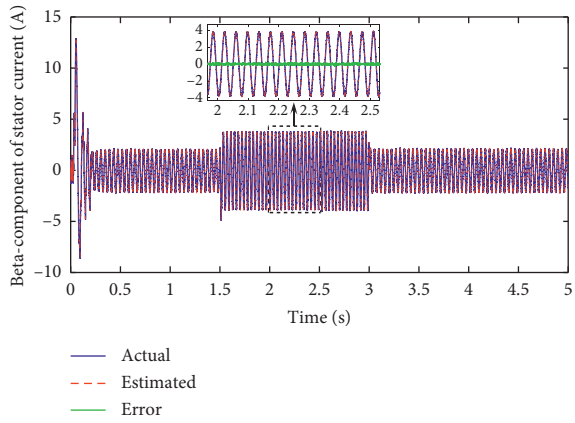


Figure 27: $\beta$-component of current for DMP VC (A).

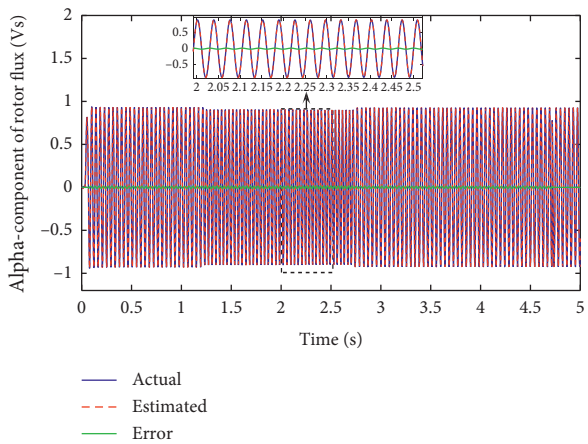


Figure 28: $\alpha$-component of flux for DMP VC (Vs).

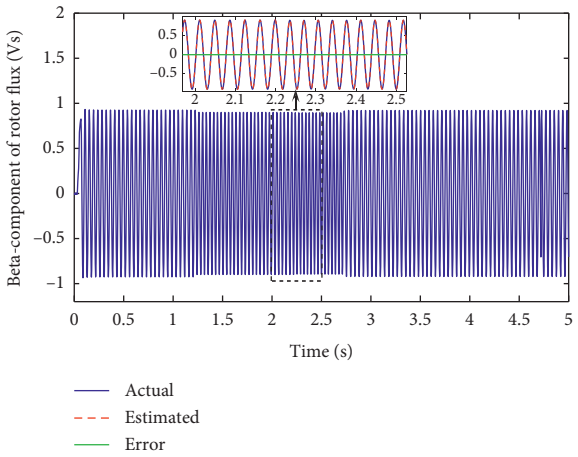


Figure 29: $\beta$-component of flux for DMP VC (Vs).

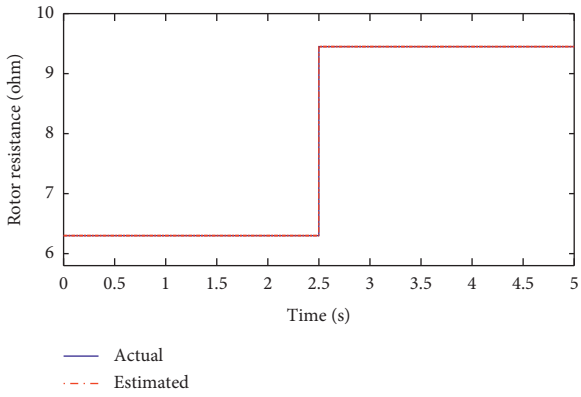


Figure 30: $R_r$ resistance variation under DMP VC ($\Omega$).

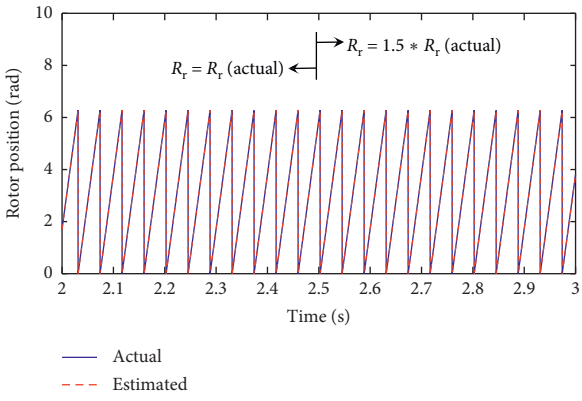


Figure 31: Rotor position under DMP VC (rad).

From Figures 42–46, the effectiveness of the proposed back-stepping observer under the MP DTC can be verified. Figure 42 reports that the estimated and actual speeds are matching each other with minimum deviation. Figures 43 and 44 show the estimated and measured ($\alpha$-$\beta$) components of stator current from which the precision of the estimation can be easily noticed. Also, the same behavior is noticed in the estimated ($\alpha$-$\beta$) components of rotor flux as shown in Figures 45 and 46.

The proposed back-stepping observer is also verifying its validity through the precise estimation of the rotor resistance and rotor position with minimum error, and this is

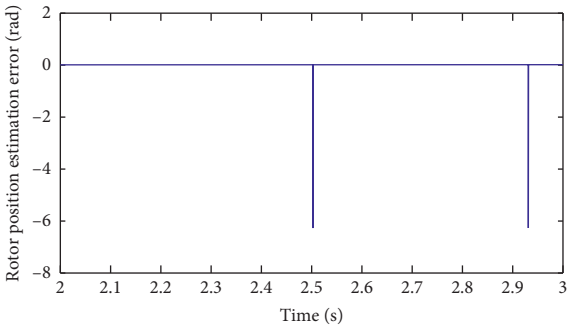


Figure 32: Rotor position error under DMP VC (rad).

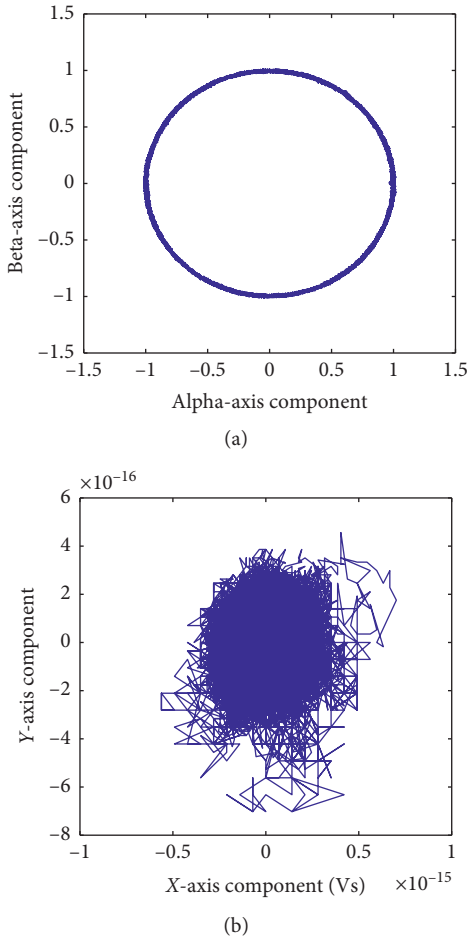


Figure 33: Stator flux loci under DMP VC.

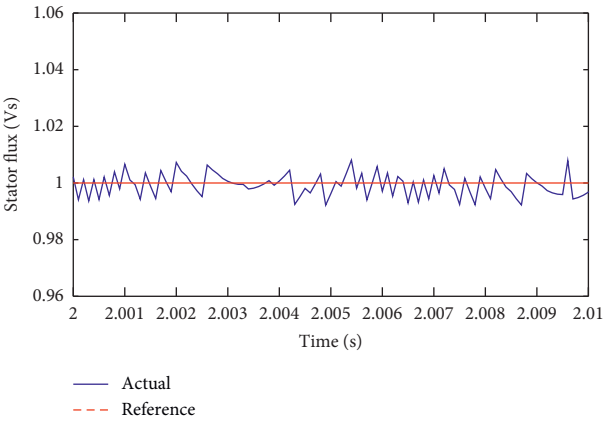


Figure 34: Stator flux ripples under DMP VC (Vs).

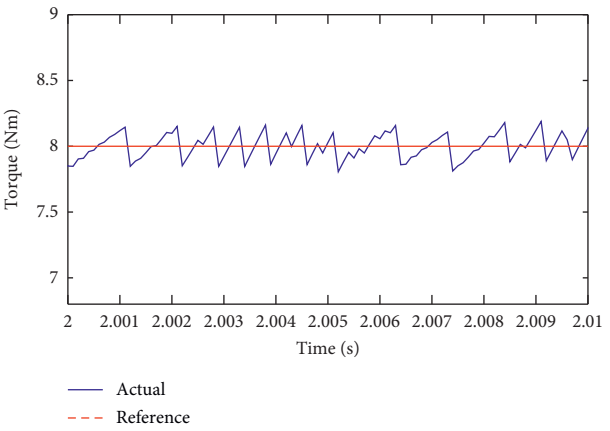


Figure 35: Torque ripples under DMP VC (Nm).

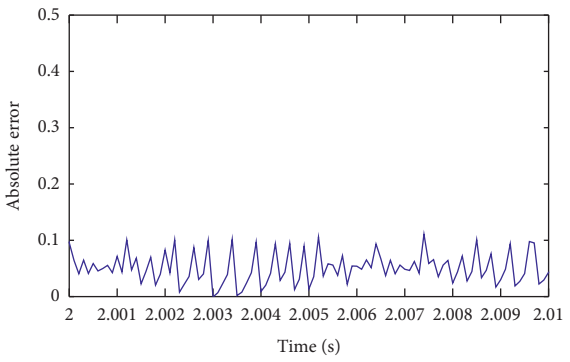


Figure 36: Absolute error under DMP VC.

illustrated in Figures 47–49. The behavior of the MP DTC can be checked through Figures 50 and 51, which show the phase "a" stator current and its FFT spectrum analysis, which gives a THD value of 6.98% of the fundamental, revealing the noticeable ripples content. This fact can be also noticed from the stator flux loci shown in Figure 52. The detailed view about the deviations of stator flux and developed torque from their references and the absolute error can be shown in Figures 53–55, respectively. The absolute error as an indication to the ripples gives a value of 0.23. Figure 56 reports the $d$-$q$ components of applied stator voltage within which the accompanied noise can be easily verified.

*6.2.2. Performance of FPIM Drive under the Proposed DMP VC (Low Speed).* The obtained results reveal the superiority of the proposed DMP VC over the MP DTC approach. Moreover, the proposed back-stepping observer is still confirming its validity in achieving high precision in the

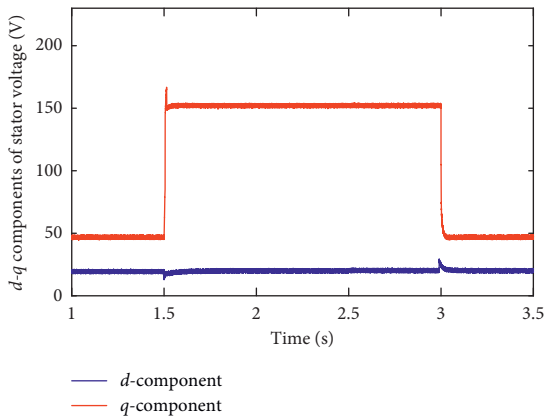


Figure 37: $d$-$q$ components of stator voltage under DMP VC (V).

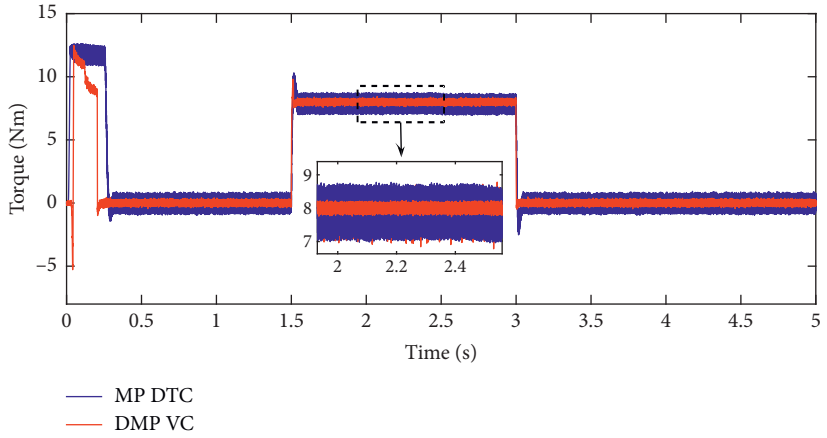


Figure 38: Torque under two control approaches at high speed operation (Nm).

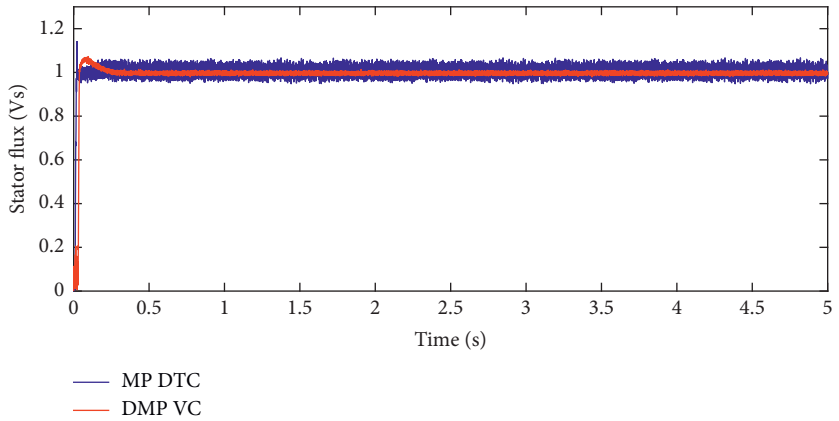


Figure 39: Stator flux under two control approaches at high speed operation (Vs).

estimation of rotor speed, stator current, rotor flux, rotor resistance, and rotor position. This fact can be observed from Figure 57, which shows the actual and estimated speed, and Figures 58 and 59, which show the measured and estimated ($\alpha$-$\beta$) components of stator current; Figures 60 and 61 show the actual and estimated values of ($\alpha$-$\beta$) components of rotor flux.

Figure 62 shows the actual and estimated rotor resistance, while Figures 63 and 64 show the measured and estimated rotor position and the position estimation error,

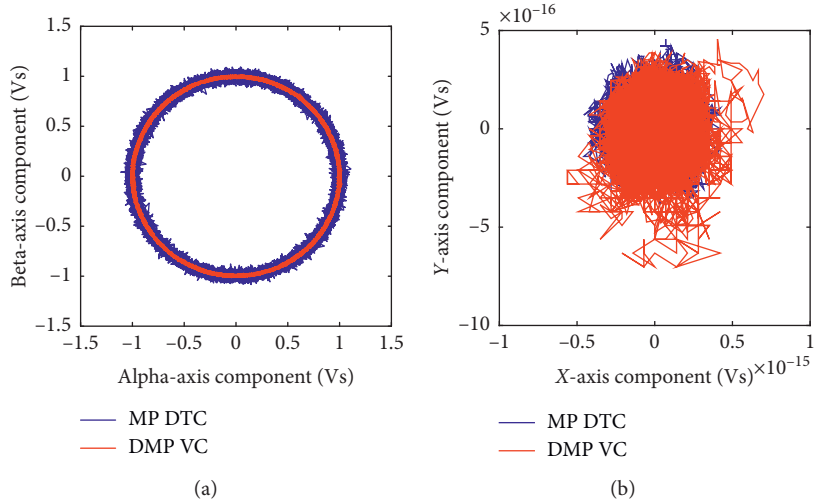


Figure 40: Stator flux loci for the two control approaches at high speed operation (Vs).

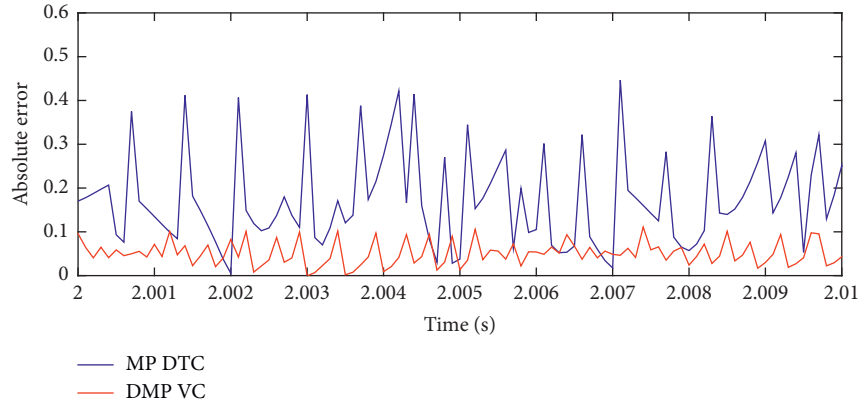


Figure 41: Absolute error for the two control approaches at high speed operation (Vs).

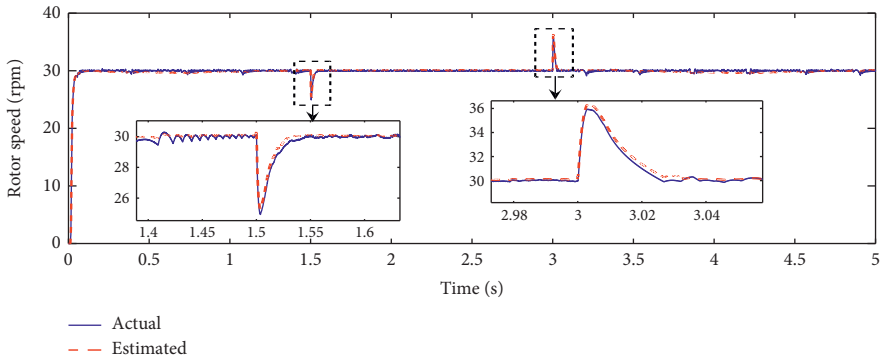


Figure 42: Rotor speed under MP DTC (rpm).

respectively. Figure 65 illustrates the stator flux loci in the ($\alpha$-$\beta$) and ($x$-$y$) planes. The superiority of the proposed DMP VC over the MP DTC in limiting the accompanied ripples can be investigated through Figures 66 and 67, which report that the stator current is accompanied with less ripples content and its FFT spectrum analysis gives a THD value of 2.04% of the fundamental, which is lower than its correspondent under the MP DTC approach. The reduced ripples with the proposed DMP VC can be also verified through Figures 68–70, which illustrate the stator flux deviation, the torque deviation, and the absolute error, respectively. The absolute error is now presenting a value of 0.042, which is

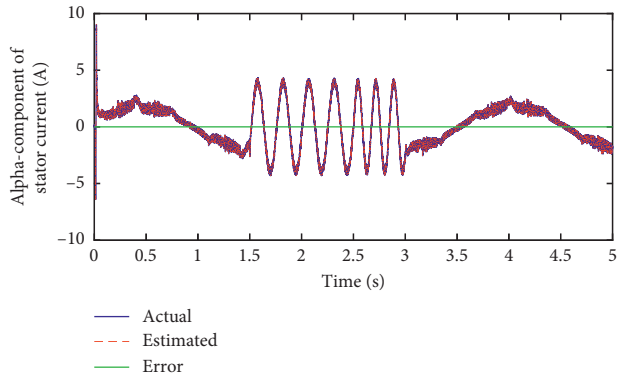


Figure 43: $\alpha$-Component of stator current for MP DTC (A).

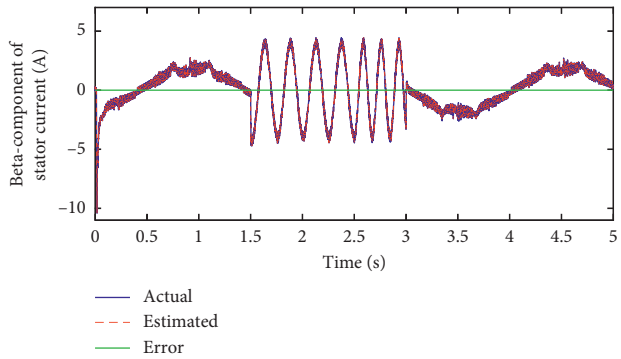


Figure 44: $\beta$-Component of stator current for MP DTC (A).

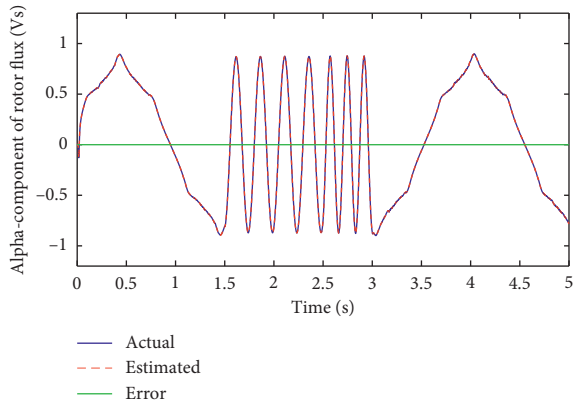


Figure 45: $\alpha$-Component of flux under MP DTC (Vs).

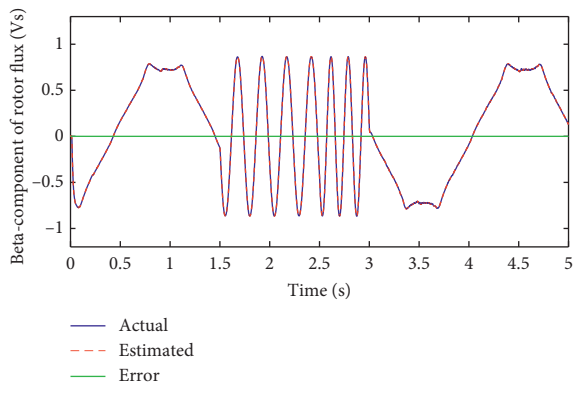


Figure 46: $\beta$-Component of flux under MP DTC (Vs).

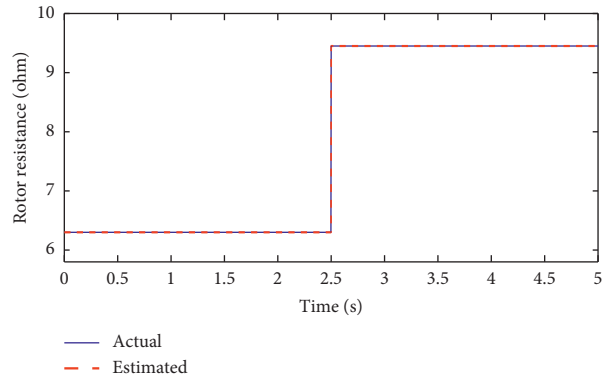


Figure 47: $R_r$ resistance variation under MP DTC (Ω).

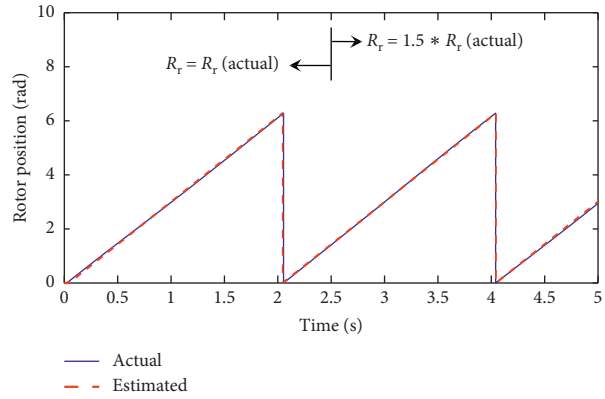


Figure 48: Rotor position under MP DTC (rad).

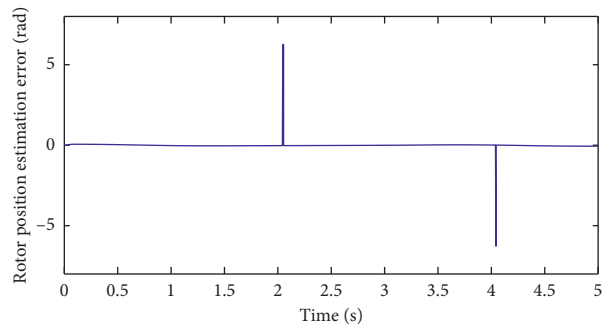


Figure 49: Rotor position error under MP DTC (rad).

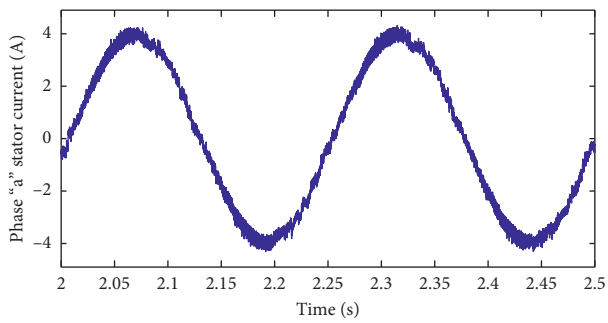


Figure 50: Phase "a" stator current for MP DTC (A).

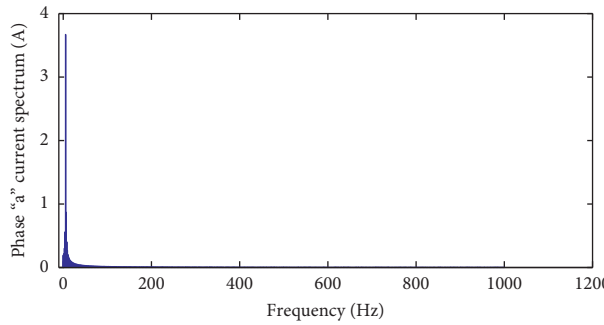


Figure 51: Phase "a" current spectrum.

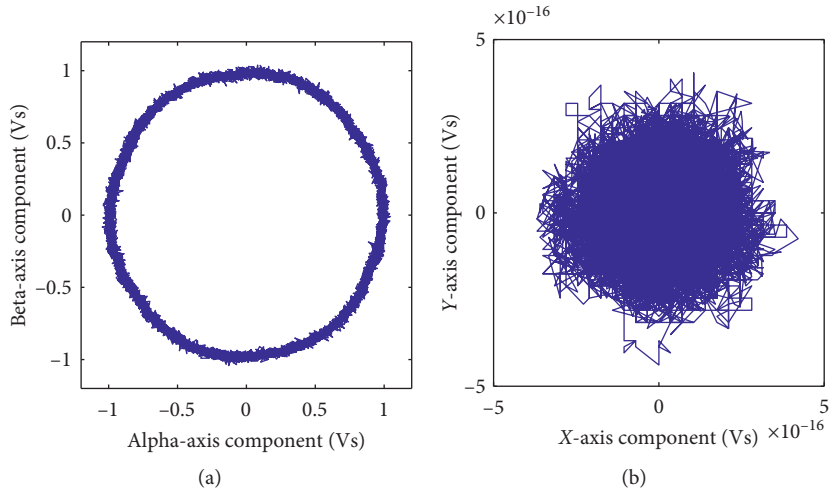


Figure 52: Stator flux loci under MP DTC.

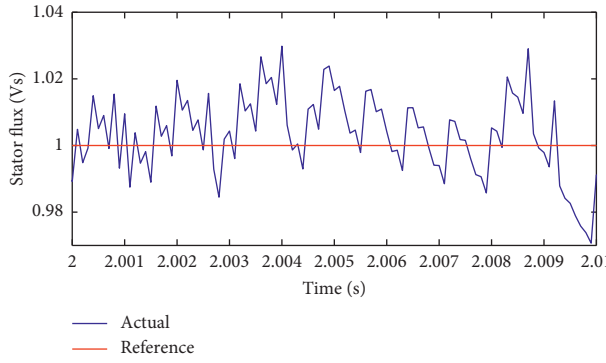


Figure 53: Stator flux ripples under MP DTC (Vs).

lower than that for the MP DTC approach. Finally, Figure 71 shows the *d*-*q* components of the applied stator voltage, which exhibit lower harmonic distortion than the MP DTC approach.

Figures 72–75 show a comparison between the two control approaches (MP DTC and proposed DMP VC) in terms of the developed torque, the stator flux magnitude, stator flux loci, and absolute error. From this comparison, it can be confirmed that the proposed DMP VC has the best performance compared with the other procedures.

The number of commutations which are developed by the inverter switches is used as a way of comparison between the three control procedures. This can be realized via utilizing the voltage index. This procedure can be

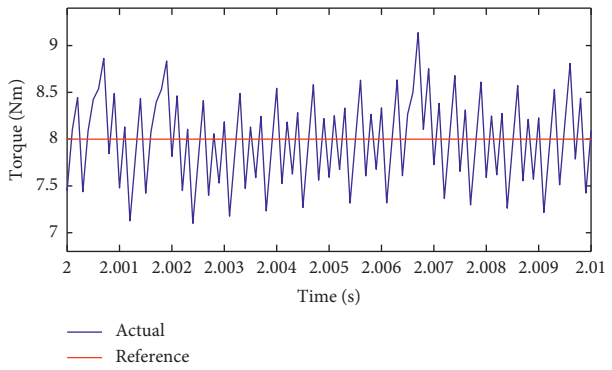


Figure 54: Torque ripples under MP DTC (Nm).

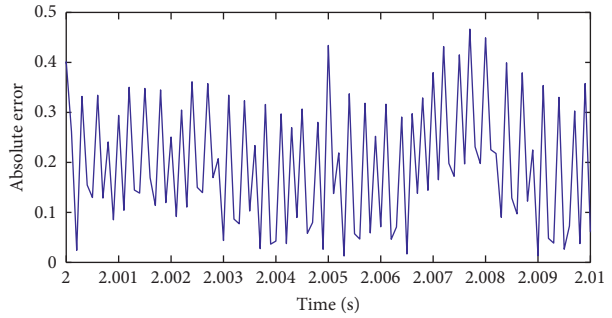


Figure 55: Absolute error under MP DTC.

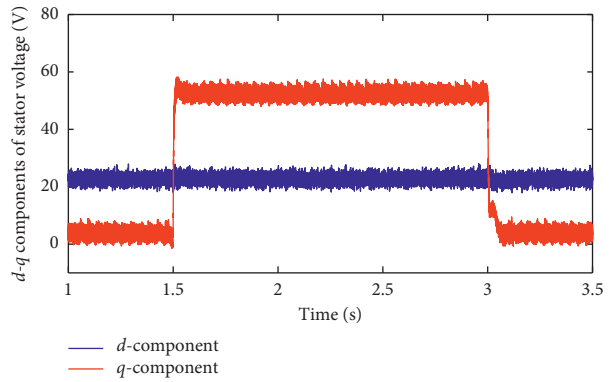


Figure 56: Stator voltage $d$-$q$ components for MP DTC (V).

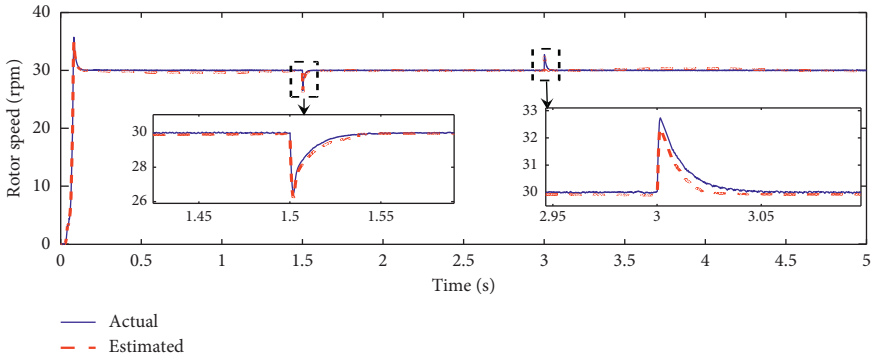


Figure 57: Rotor speed under DMP VC (rpm).

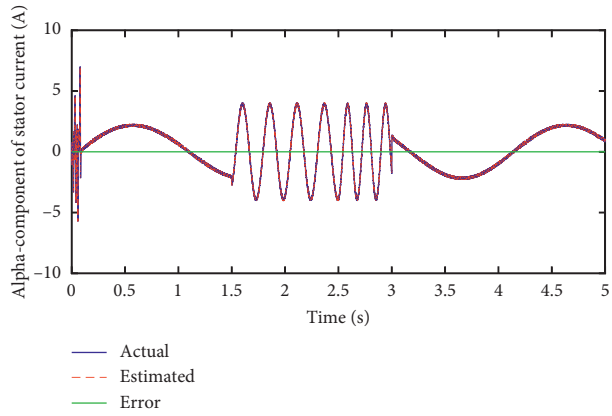


Figure 58: $\alpha$-Component of stator current for DMP VC (A).

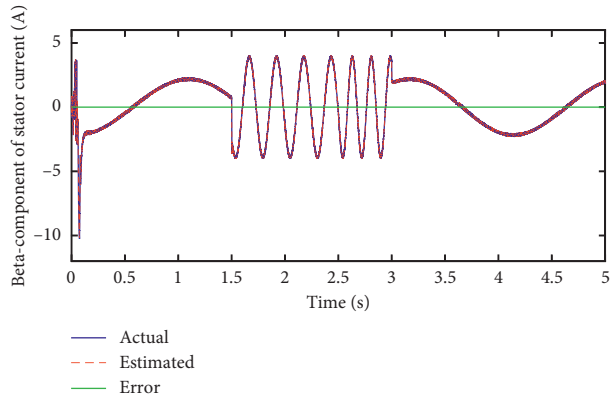


Figure 59: $\beta$-Component of stator current for DMP VC (A).

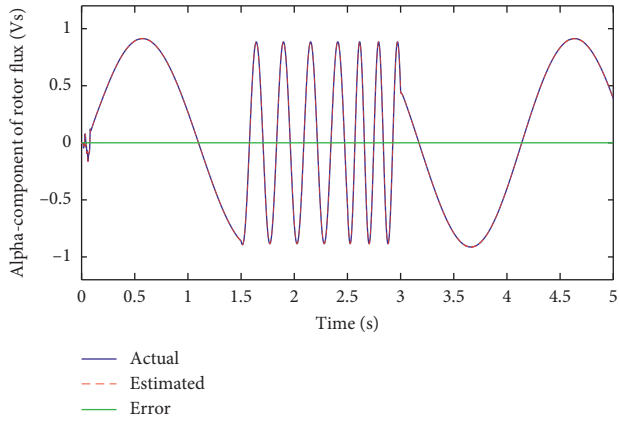


Figure 60: $\alpha$-Component of flux under DMP VC (Vs).

realized due to the fact that, for each voltage index variation, the switches in the five branches ($A$, $B$, $C$, $D$, and $E$) change their states. Thus, if the successive switching states are identified and the switching changes are stored as a binary change (0 or 1), then, by summing all of these changes, the definite number of commutations can be evaluated.

Then, the number of commutations for high speed and low speed operations for the two control procedures can be obtained as in Tables 2 and 3, respectively.

From the obtained results in Tables 2 and 3, it can be concluded that the DMP VC is developing the lowest number of commutations, and this can be referred to the simple form of (27), which does not involve any term that

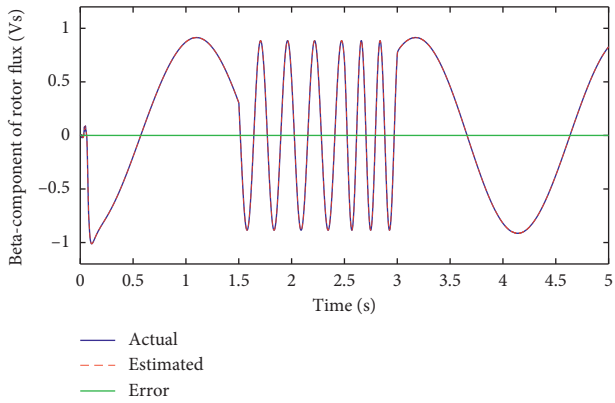


Figure 61: $\beta$-Component of flux under DMP VC (Vs).

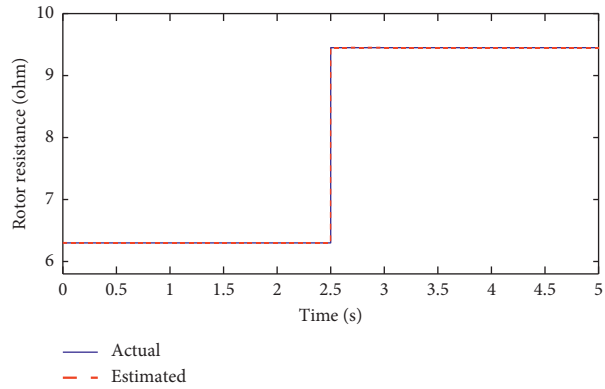


Figure 62: $R_r$ variation under DMP VC ($\Omega$).

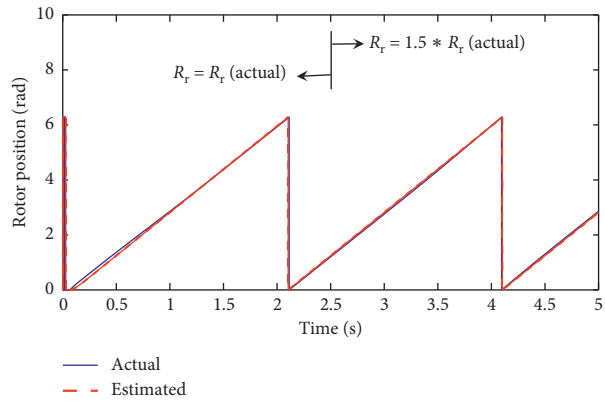


Figure 63: Rotor position under DMP VC (rad).

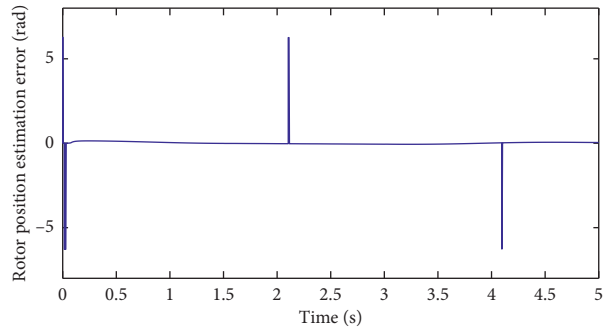


Figure 64: Rotor position error under DMP VC (rad).

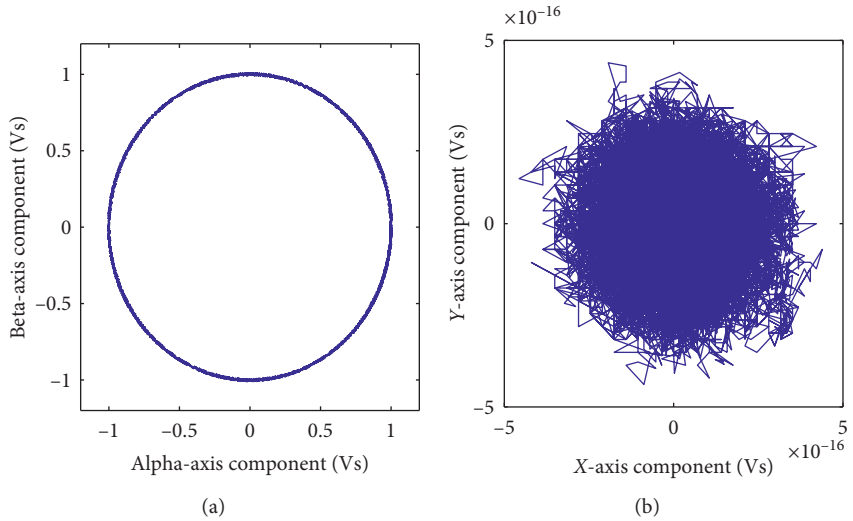


Figure 65: Stator flux loci under DMP VC.

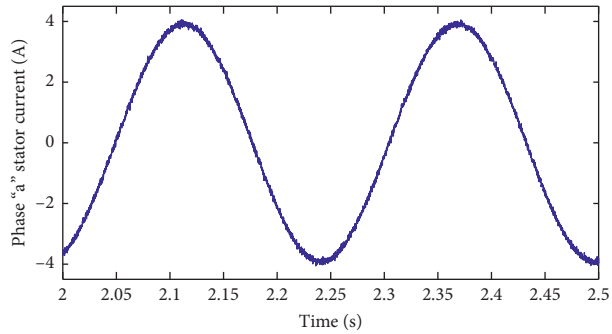


Figure 66: Phase "a" stator current for DMP VC (A).

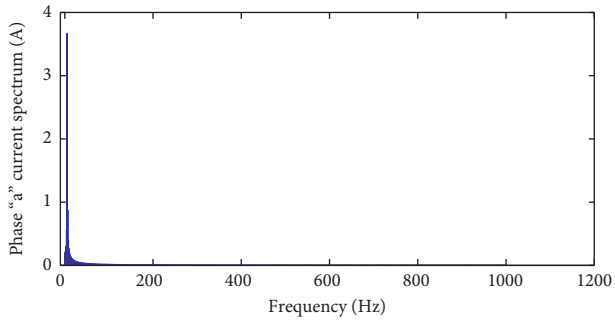


Figure 67: Phase "a" stator current spectrum.

needs to be estimated as in the cost functions used by the MP DTC.

Another form of comparison can be presented through evaluating the switching losses. These losses can be estimated using the commutations number and switching frequencies ($f_{sw}$) as follows.

The average switching losses ($P_{sw}$) for the IGBTs per switching interval can be calculated by

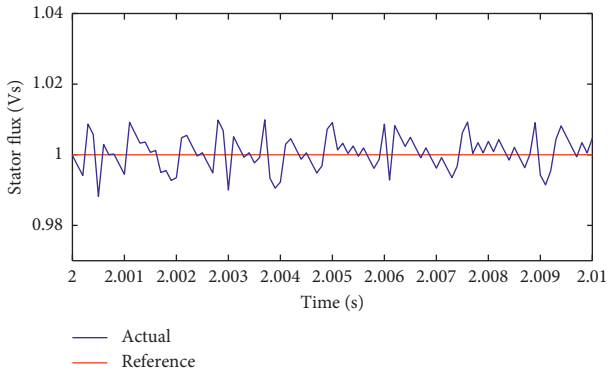


Figure 68: Stator flux ripples under DMP VC (Vs).

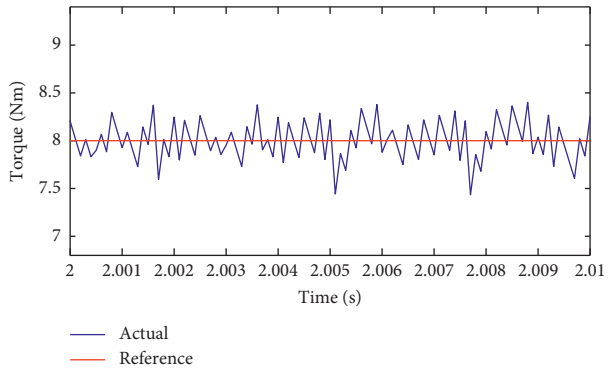


Figure 69: Torque ripples under DMP VC (Nm).

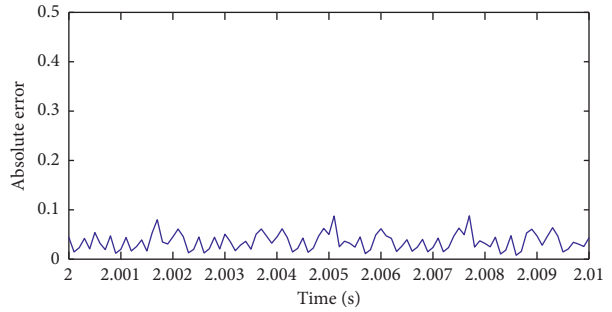


Figure 70: Absolute error under DMP VC.

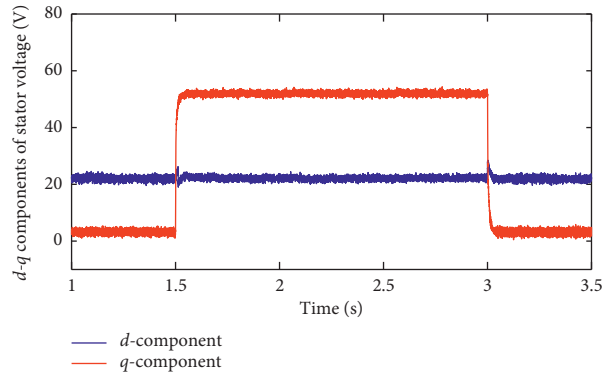


Figure 71: Stator voltage $d$-$q$ components for DMP VC (V).

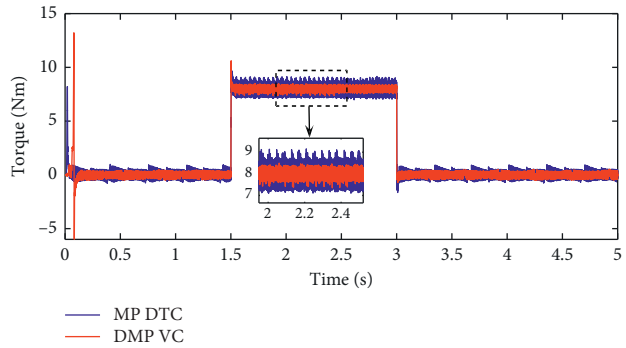


Figure 72: Torque under two control approaches at low speed operation (Nm).

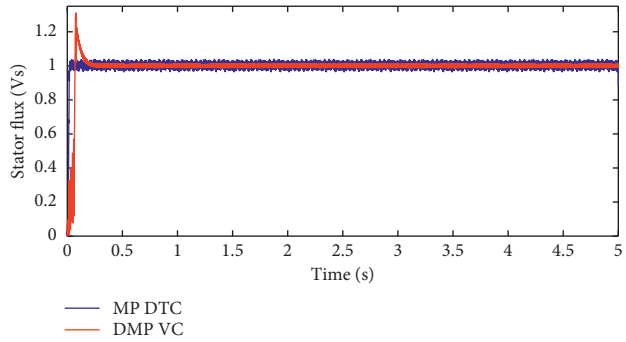


Figure 73: Stator flux under two control approaches at low speed operation (Vs).

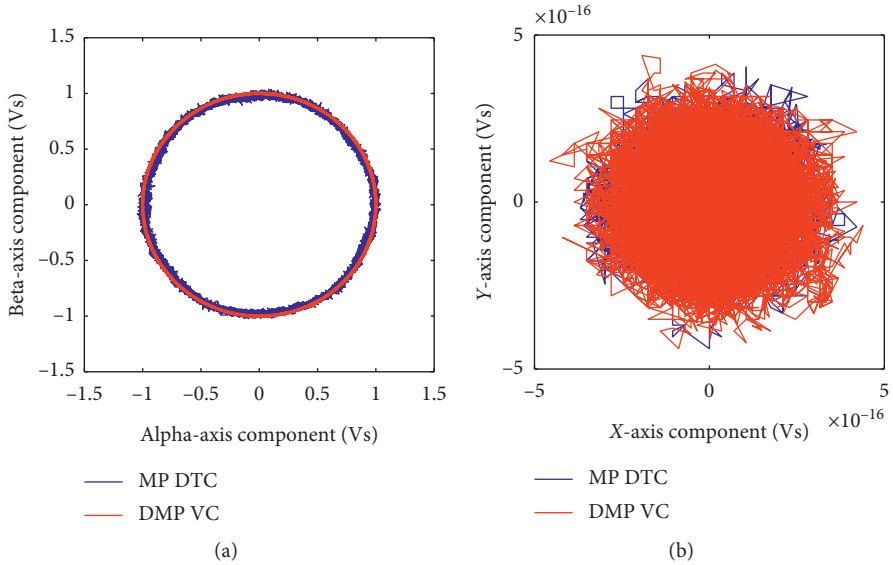


Figure 74: Stator flux loci for the two control approaches at low speed operation (Vs).

$$P_{sw} = \frac{E_{on} + E_{off}}{\pi} f_{sw}, \tag{62}$$

where $E_{on}$ and $E_{off}$ are the on and off energy losses of the IGBT switches, respectively. These two values are calculated as functions of the developed commutations, the emitter's current, and collector-emitter voltage. The following comparison is obtained for high and low speed operation.

The comparison can be also performed in terms of the execution time taken by each control cycle for the two control procedures. This can be illustrated in Tables 4 and 5.

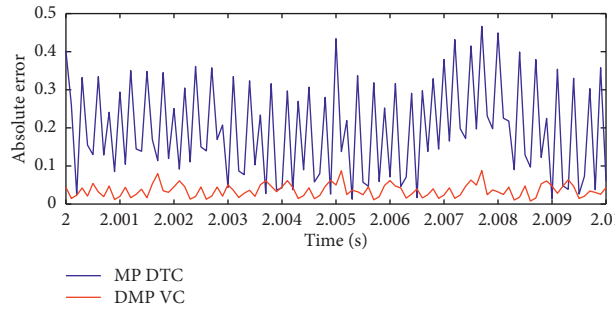


Figure 75: Absolute error for the two control approaches at low speed operation (Vs).

Table 2: Comparison in terms of number of commutations at high speed operation.

| | No. of commutations | Switching frequency |
|---|---|---|
| MP DTC | 8674 | 1.44 |
| Proposed DMP VC | 4659 | 776 |

Table 3: Comparison in terms of number of commutations at low speed operation.

| | No. of commutations | Switching frequency (kHz) |
|---|---|---|
| MP DTC | 3513 | 586 |
| Proposed DMP VC | 1684 | 281 |

Table 4: Comparison in terms of computation time at high speed operation.

| | |
|---|---|
| MP DTC | 19.1 $\mu$s |
| Proposed DMP VC | 8.9 $\mu$s |

Table 5: Comparison in terms of computation time at low speed operation.

| | |
|---|---|
| MP DTC | 8.2 $\mu$s |
| Proposed DMP VC | 4.3 $\mu$s |

Table 6: Comparison in terms of number of switching power losses at high speed operation.

| | |
|---|---|
| MP DTC | 104.025 W |
| Proposed DMP VC | 55.906 W |

Table 7: Comparison in terms of number of switching power losses at low speed operation.

| | |
|---|---|
| MP DTC | 42.106 W |
| Proposed DMP VC | 20.207 W |

From the data of Tables 4–7, it can be realized that the proposed DMP VC approach has the minimum switching power losses compared with the MP DTC approach, and this was expected due to the reduction in the number of commutations for the proposed DMP VC approach. Also the time taken for execution can be considered as a translation to the number of commutations as can be noticed that the time taken by the proposed DMP VC is the shortest time, which means the lowest number of commutations performed in each cycle.

## 7. Conclusion

The paper has presented a novel direct model predictive voltage control (DMP VC) approach for a sensorless five-phase induction motor (FPIM) drive. An effective back-stepping observer is designed for estimating rotor speed, stator current, rotor flux, and rotor resistance. The performance of the FPIM drive is tested with the proposed DMP VC approach for a wide range of speed operations. The performance of the FPIM with the proposed DMP VC is compared with the performance of the well-known model predictive direct torque (MP DTC) approach. The obtained results confirm and emphasize the priority of the proposed DMP VC approach over the MP DTC control procedure in limiting the accompanied noise in the controlled variables, thus enhancing the dynamic performance of the drive. Moreover, the proposed back-stepping observer's effectiveness has been verified for all speed ranges. Based upon the detailed and comprehensive analysis presented in this paper, it is realized that the proposed DMP VC can be utilized as a better alternative to the MP DTC control approach.

## Data Availability

The data used to support the findings of this study are available from the corresponding author upon request.

## Conflicts of Interest

The authors declare that they have no conflicts of interest.

## Acknowledgments

This work was supported by Lac Hong University.

## References

[1] E. Levi, "Multiphase electric machines for variable-speed applications," *IEEE Transactions on Industrial Electronics*, vol. 55, no. 5, pp. 1893–1909, 2008.

[2] Z. Liu, Y. Li, and Z. Zheng, "A review of drive techniques for multiphase machines," *China Electrotechnical Society*

*Transactions on Electrical Machines and Systems*, vol. 2, no. 2, pp. 243–251, 2018.

[3] A. G. Yepes, F. Baneira, J. Malvar et al., "Selection criteria of multiphase induction machines for speed-sensorless drives based on rotor slot harmonics," *IEEE Transactions on Industrial Electronics*, vol. 63, no. 8, pp. 4663–4673, 2016.

[4] N. K. Nguyen, F. Meinguet, E. Semail, and X. Kestelyn, "Fault-tolerant operation of an open-end winding five-phase PMSM drive with short-circuit inverter fault," *IEEE Transactions on Industrial Electronics*, vol. 63, no. 1, pp. 595–605, 2016.

[5] W. N. W. A. Munim, M. J. Duran, H. S. Che, M. Bermúdez, I. González-Prieto, and N. A. Rahim, "A unified analysis of the fault tolerance capability in six-phase induction motor drives," *IEEE Transactions on Power Electronics*, vol. 32, no. 10, pp. 7824–7836, 2017.

[6] I. González-Prieto, M. J. Duran, and F. J. Barrero, "Fault-tolerant control of six-phase induction motor drives with variable current injection," *IEEE Transactions on Power Electronics*, vol. 32, no. 10, pp. 7894–7903, 2017.

[7] R. Bojoi, A. Cavagnino, A. Tenconi, and S. Vaschetto, "Control of shaft-line-embedded multiphase starter/generator for aero-engine," *IEEE Transactions on Industrial Electronics*, vol. 63, no. 1, pp. 641–652, 2016.

[8] E. Levi, R. Bojoi, F. Profumo, H. A. Toliyat, and S. Williamson, "Multiphase induction motor drives - a technology status review," *IET Electric Power Applications,*vol. 1, no. 4, pp. 489–516, 2007.

[9] R. Bojoi, A. Cavagnino, M. Cossale, and A. Tenconi, "Multiphase starter generator for a 48 V mini-hybrid powertrain: design and testing," *IEEE Transactions on Industry Applications*, vol. 52, no. 2, pp. 1750–1758, 2016.

[10] M. J. Duran, F. Salas, and M. R. Arahal, "Bifurcation analysis of five-phase induction motor drives with third harmonic injection," *IEEE Transactions on Industrial Electronics*, vol. 55, no. 5, pp. 2006–2014, 2008.

[11] H. Guzman, F. Barrero, and M. J. Duran, "IGBT-gating failure effect on a fault-tolerant predictive current-controlled five-phase induction motor drive," *IEEE Transactions on Industrial Electronics*, vol. 62, no. 1, pp. 15–20, 2015.

[12] J. A. Riveros, F. Barrero, E. Levi, M. J. Durán, S. Toral, and M. Jones, "Variable-speed five-phase induction motor drive based on predictive torque control," *IEEE Transactions on Industrial Electronics*, vol. 60, no. 8, pp. 2957–2968, 2013.

[13] B. Tian, Q.-T. An, J.-D. Duan, D.-Y. Sun, L. Sun, and D. Semenov, "Decoupled modeling and nonlinear speed control for five-phase PM motor under single-phase open fault," *IEEE Transactions on Power Electronics*, vol. 32, no. 7, pp. 5473–5486, 2017.

[14] H. Echeikh, R. Trabelsi, A. Iqbal, N. Bianchi, and M. F. Mimouni, "Comparative study between the rotor flux oriented control and non-linear backstepping control of a five-phase induction motor drive—an experimental validation," *IET Power Electronics*, vol. 9, no. 13, pp. 2510–2521, 2016.

[15] L. Zheng, J. E. Fletcher, B. W. Williams, and X. He, "A novel direct torque control scheme for a sensorless five-phase induction motor drive," *IEEE Transactions on Industrial Electronics*, vol. 58, no. 2, pp. 503–513, 2011.

[16] Y. N. Tatte and M. V. Aware, "Direct torque control of five-phase induction motor with common-mode voltage and current harmonics reduction," *IEEE Transactions on Power Electronics*, vol. 32, no. 11, pp. 8644–8654, 2017.

[17] J. A. Riveros, J. Prieto, F. Barrero, S. Toral, M. Jones, and E. Levi, "Predictive torque control for five-phase induction motor drives," in *Proceedings of the IECON 2010—36th Annual Conference on IEEE Industrial Electronics Society*, pp. 2467–2472, Glendale, AZ, USA, 2010.

[18] A. Pal, S. Das, and A. K. Chattopadhyay, "An improved rotor flux space vector based MRAS for field-oriented control of induction motor drives," *IEEE Transactions on Power Electronics*, vol. 33, no. 6, pp. 5131–5141, 2018.

[19] M. R. Khan, A. Iqbal, and M. Ahmad, "MRAS-based sensorless control of a vector controlled five-phase induction motor drive," *Electric Power Systems Research*, vol. 78, no. 8, pp. 1311–1321, 2008.

[20] D. Bao, H. Wang, X. Wang, and C. Zhang, "Sensorless speed control based on the improved Q-MRAS method for induction motor drives," *Energies*, vol. 11, no. 1, p. 235, 2018.

[21] C. Lascu, I. Boldea, and F. Blaabjerg, "Direct torque control of sensorless induction motor drives: a sliding-mode approach," *IEEE Transactions on Industry Applications*, vol. 40, no. 2, pp. 582–590, 2004.

[22] Y. Geng, Z. Lai, Y. Li, D. Wang, R. Chen, and P. Zheng, "Sensorless fault-tolerant control strategy of six-phase induction machine based on harmonic suppression and sliding mode observer," *IEEE Access*, vol. 7, pp. 110086–110102, 2019.

[23] Y. Zhonggang, L. Guoyin, Z. Yanqing, L. Jing, S. Xiangdong, and Z. Yanru, "A speed and flux observer of induction motor based on extended Kalman filter and Markov chain," *IEEE Trans. Power Electron.*vol. 32, no. 9, pp. 7096–7117, 2017.

[24] Y.-D. Yoon and S.-K. Sul, "Sensorless control for induction machines based on square-wave voltage injection," *IEEE Transactions on Power Electronics*, vol. 29, no. 7, pp. 3637–3645, 2014.

[25] L. Sheng, G. Xiaojie, and Z. Lanyong, "Robust adaptive backstepping sliding mode control for six-phase permanent magnet synchronous motor using recurrent wavelet fuzzy neural network," *IEEE Access*, vol. 5, pp. 14502–14515, 2017.

[26] S. M. J. Rastegar Fatemi, N. R. Abjadi, J. Soltani, and S. Abazari, "Speed sensorless control of a six-phase induction motor drive using backstepping control," *IET Power Electronics*, vol. 7, no. 1, pp. 114–123, 2014.

[27] D. P. Marcetic and S. N. Vukosavic, "Speed-sensorless AC drives with the rotor time constant parameter update," *IEEE Transactions on Industrial Electronics*, vol. 54, no. 5, pp. 2618–2625, 2007.

[28] J. Listwan and K. Pieńkowski, "Field-oriented control of five-phase induction motor with open-end stator winding," *Archives of Electrical Engineering*, vol. 65, no. 3, pp. 395–410, 2016.

[29] M. S. Alam and M. R. Khan, "Stability analysis of a five-phase induction motor drive using variable frequency technique," *Universal Journal of Electrical and Electronic Engineering*, vol. 4, no. 5, pp. 120–128, 2016.

[30] A. Derdiyok, M. K. Guven, H. Rehman, and L. Xu, "A new approach to induction machine flux and speed observer with online rotor time constant estimation," in *Proceedings of the IEMDC 2001. IEEE International Electric Machines And Drives Conference (Cat. No. 01EX485)*, pp. 102–107, Cambridge, MA, USA, June 2001.

[31] A. Derdiyok, "A novel speed estimation algorithm for induction machines," *Electric Power Systems Research*, vol. 64, no. 1, pp. 73–80, 2003.